CALORIMETRIC STUDIES

of

SILVER INTERCALATED TITANIUM DISULPHIDE

by

GARY M. JACKLE

B.Sc., Simon Fraser University, 1980

A THESIS SUBMITTED IN PARTIAL FULFILLMENT OF

THE REQUIREMENTS FOR THE DEGREE OF

MASTER OF SCIENCE

in the Department

of

Physics

SIMON FRASER UNIVERSITY

December 1985

APPROVAL

Name: Gary M. Jackle

Degree: Master of Science

Title of Thesis: Calorimetric Studies of Silver Intercalated Titanium Disulphide

Examining Committee:

Chairman: K. S. Viswanathan

J. C. Irwin
Senior Supervisor

B. P. Clayman

R. F. Frindt

M. Plischke
External Examiner
Physics Department, SFU

Date Approved: December 20, 1985

PARTIAL COPYRIGHT LICENSE

I hereby grant to Simon Fraser University the right to lend my thesis, project or extended essay (the title of which is shown below) to users of the Simon Fraser University Library, and to make partial or single copies only for such users or in response to a request from the library of any other university, or other educational institution, on its own behalf or for one of its users. I further agree that permission for multiple copying of this work for scholarly purposes may be granted by me or the Dean of Graduate Studies. It is understood that copying or publication of this work for financial gain shall not be allowed without my written permission.

Title of Thesis/Project/Extended Essay

CALORIMETRIC STUDIES OF SILVER

INTERCALATED TITANIUM DISULPHIDE

Author:

(signature)

GARY JACKLE

(name)

June 4, 1986

(date)

ABSTRACT

The order-disorder transition of the silver atoms in the intercalation compound Ag_xTiS_2 has been investigated using differential scanning calorimetry. Measurements were carried out for silver concentrations in the range $0 < x \leq 0.5$ and for temperatures in the region $150\ K < T < 650\ K$. The Ag_xTiS_2 samples used in this work were prepared by thermally intercalating Ag into TiS_2 powders. The intercalated powders were calibrated using X-ray fluorescence and X-ray diffraction techniques. Values obtained for the critical temperature Tc were in good agreement with previously reported results and there was no measurable hysteresis in the transition. The latter result is consistent with the predicted second order nature of the transition. Results were also obtained for the specific heat of pure TiS_2 and for the intercalation compounds Ag_xTiS_2. The measured variation of the specific heat of the Ag_xTiS_2 samples near Tc has been compared to the predictions of a two-dimensional theoretical model.

TABLE OF CONTENTS

PAGE

PAGE

LIST OF FIGURES

CHAPTER 1

INTRODUCTION

Layered compounds have been and are of interest to scientists because of the anisotropy of their physical properties that is observed in configurations alternately parallel and perpendicular to the basal plane. Interest in new and less expensive forms of energy has resulted in economic incentives being made available for energy related research and a significant portion of this research has been directed to the study of layered compounds. For example, research involving the transition metal dichalcogenides has shown that these materials may be excellent candidates as cathodes in high energy density, light weight electro-intercalation batteries (1,2,3,4,5,6,7). When a cathode (made of one of the transition metal dichalcogenides) is immersed in a suitable electrolyte with an appropriate counter electrode the ions in solution migrate into the cathode by means of a highly reversible topochemical (chemical bonds are neither formed or broken) reaction producing an EMF as high as a few volts. Other areas of research (8) point to the potential use of transition metal dichalcogenides as catalysts in hydrodesulfurization processes (removal of sulfur contaminants from petroleum products). The sulfur which contaminates fossil fuels tends to combine with hydrogen and oxygen in the atmosphere resulting in compounds of major environmental concern.

The transition metal dichalcogenides are also of interest to scientists because of the quasi-two-dimensional properties for atoms inserted in the region between the layers of the host dichalcogenide. A large variety of ions and molecules can be inserted or intercalated between the layers because of the relatively weak interlayer bonding. The intercalate is therefore constrained to a nearly two-dimensional region and thus provides a quasi-two-dimensional system whose physical properties can be studied. In particular the intercalated atoms have been observed to undergo order-disorder transitions in a number of different systems (3, 5, 14, 18, 19, 20, 21, 23, 36).

The order-disorder transitions in graphite intercalated compounds have attracted a great deal of attention. Parry and co-workers (10) were among the first to explore the ordering of intercalate species in graphite. Many others have continued these investigations. Clarke et. al. (24) used X-ray diffraction to investigate the order-disorder transition of cesium intercalated graphite, finding a discontinuity in the integrated intensity of various X-ray peaks around the order-disorder temperature T_C, and Zabel et. al. (11) used the same technique to investigate the ordering of potassium in graphite. Leung and co-workers (12) were the first to report the infrared optic modes for stage 1 and stage 2 graphite intercalated with potassium, rubidium and

cesium. Neutron diffraction studies were carried out on the same compounds by Zabel et. al. (13) who measured the [001] longitudinal acoustical and optical phonon branches and subsequently determined the force constants. They (13) found that the range and strength of the interplanar interaction increases upon intercalation with alkali atoms.

Intercalate ordering has been observed in the intercalated layered dichalcogenide compounds. Features of the potential versus intercalate concentration curves (3) of Li_xTiS_2 were interpreted by Thompson (3, 4) as evidence that the lithium ions ordered between the TiS_2 layers. Berlinsky et. al. (46) modeled the Li_xTiS_2 system with a lattice gas model and their results appeared to support the suggestion that the lithium atoms ordered for certain intercalate concentrations (x). This ordering has never been observed experimentally in the Li_xTiS_2 system despite the fact that an exhaustive search has been carried out. Investigations have been made at temperatures between 4 K and 300 K using X-ray diffraction techniques (23), neutron scattering (48, 51), light scattering (22), electron microscopy (21), and electrochemical methods (47, 49). It is now generally agreed that lithium does not order in TiS_2 above 4.2 K. On the other hand Dahn and McKinnon (56, 64) have recently obtained indirect evidence from electrochemical measurements for the ordering of lithium in TaS_2. They have also suggested that second neighbour interactions may be responsible for

suppressing the order-disorder transition in the Li_xTiS_2 system.

Intercalate ordering has been much easier to observe in other dichalcogenide intercalation systems. For example, Boswell et. al (18) used electron diffraction to observe the ordering of copper atoms in Cu_xNbS_2 and Ridder et. al. (20) used electron microscopy to investigate the ordering of copper atoms in Cu_xNbS_2 and Cu_xTaS_2. The ordering of iron atoms in Fe_xNbS_2 was also studied by Boswell et. al. (19) as a function of temperature and composition using electron diffraction techniques.

Ag_xTiS_2 has been one of the most thoroughly investigated of the transition metal dichalcogenide intercalation compounds. The silver atom has a pseudo-alkali atomic structure having one electron in the outermost S-shell making it similar to the alkali metal atom lithium and yet is relatively inert compared to lithium. The Ag_xTiS_2 system is thus relatively easy to prepare and quite stable in a normal environment. Silver also has quite large X-ray and electron scattering cross-sections and experimental information is thus much easier to obtain from Ag_xTiS_2 than from a lithium intercalated compound. The pseudo-alkali properties of silver also suggest that many of the results obtained from Ag_xTiS_2 system will be applicable to the technologically more important Li_xTiS_2 compound.

The first observation of an order-disorder transition in Ag_xTiS_2 was made by Unger et. al. (21) who carried out Raman scattering and electron diffraction experiments on an electro-intercalated Ag_xTiS_2 sample. They found that new Raman modes appeared in the spectra as the temperature was reduced and they attributed these modes to the formation of a Ag-superlattice within the TiS_2 lattice. In addition they observed the Ag-superlattice directly in electron diffraction patterns.

Leonelli et. al. (22) and Plischke et. al. (25) investigated the temperature and silver concentration dependence of the order-disorder transition in Ag_xTiS_2 using Raman scattering experiments. They observed a continuous, apparently second order, transition and obtained excellent agreement with the predictions of a two-dimensional lattice gas model. The order-disorder transition temperature for $Ag_{0.33}TiS_2$ was estimated from Raman scattering experiments to be T_C = 300 K. The continuous variation of the square of the order parameter indicated that the transition was second order but definitive conclusions about the transition could not be made because data could not be obtained close to the critical temperature T_C.

In an effort to confirm the two-dimensional and second order nature of the transition Suter et. al. (23) carried out X-ray diffraction experiments on a thermally grown sample of $Ag_{0.33}TiS_2$. They found that the transition appeared to be

second order due to the continuous variation of the Bragg peak intensities and did not find any "cross-over" to three dimensional behaviour. They also found a somewhat lower transition temperature (265 K) than was obtained (300 K) for the electro-intercalated compounds studied in the Raman scattering experiments. Gerards et. al. (65) also came to the conclusion that the order-disorder transition was second order in nature and occurs at T_C = 301 K based on a series of X-ray and electrochemical measurements on a $Ag_{0.33}TiS_2$ sample grown by vapour transport.

This work represents an effort to obtain more definitive and complementary information on the nature of the order-disorder transition in Ag_xTiS_2, and in this thesis the results of differential scanning calorimetry experiments carried out on thermally intercalated Ag_xTiS_2 powders are presented. The experiments were carried out on samples with nominal intercalate concentrations $0 < x < 0.6$ and for temperatures between 100 K and 600 K. Chapter 2 of this thesis reviews the properties of TiS_2 crystals and describes the preparation of the TiS_2 powders and the intercalation process. Chapter 3 describes the X-ray diffraction and X-ray fluorescence techniques that were used as diagnostic tools in sample characterization. Chapter 4 reviews the Differential Scanning Calorimetry techniques. Chapter 5 presents the results of the calorimetry measurements. These measurements did not reveal any hysteresis in the transition, a result

that is in agreement with the previous assertions of the second-order nature of the transition. The variation of the specific heat near T_C is thus obtained from the measurements and the results are compared to theoretical predictions obtained by Schick and Walker (52) who used renormalization group methods for atoms adsorbed on a substrate. This dicussion of the results is contained in Chapter 6 along with the conclusions arising from this work.

CHAPTER 2

SAMPLE PREPARATION

2-1 Transition Metal Dichalcogenides

TiS_2 is a member of the family of transition metal dichalcogenide (MX_2) compounds that exist as layered structure crystals consisting of combinations of a transition metal (M) from Groups IV, V or VI of the periodic table with a chalcogen (X) chosen from the elements S, Se, Te and Ta. The layers consist of planes of transition metal atoms (M) sandwiched between two hexagonally packed planes of chalcogenide atoms (X), (Fig. 1). The six-fold coordination of the chalcogenide atoms around the transition metal atoms occurs primarily in either a trigonal anti-prism (1T) configuration (Fig. 2) or a trigonal prism (2H) configuration (Fig. 3). The structure of these materials results in their physical properties being very anisotropic and the anisotropy is enhanced by intercalation. For example, Silbernagel et. al. (48) found that expansion of the TiS_2 lattice parameters parallel to the a axis is an order of magnitude less than the expansion parallel to the c axis when lithium is added to the host TiS_2 crystal. MoS_2 is the only transition metal dichalcogenide that occurs naturally in appreciable quantities but the other transition metal dichalcogenides may be easily grown, usually by chemical vapor transport methods (27). A more complete description of

Figure 1

Hexagonal layered structure of TiS_2.

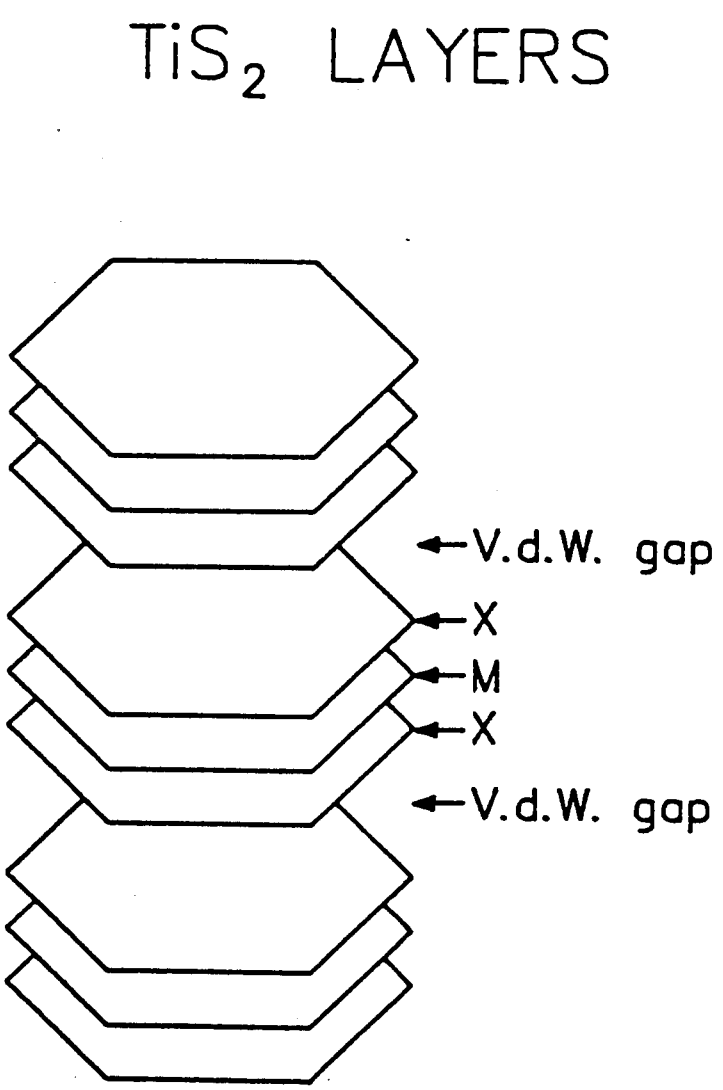

Figure 2

1-T coordination of chalcogen atoms with respect to the transition metal atom.

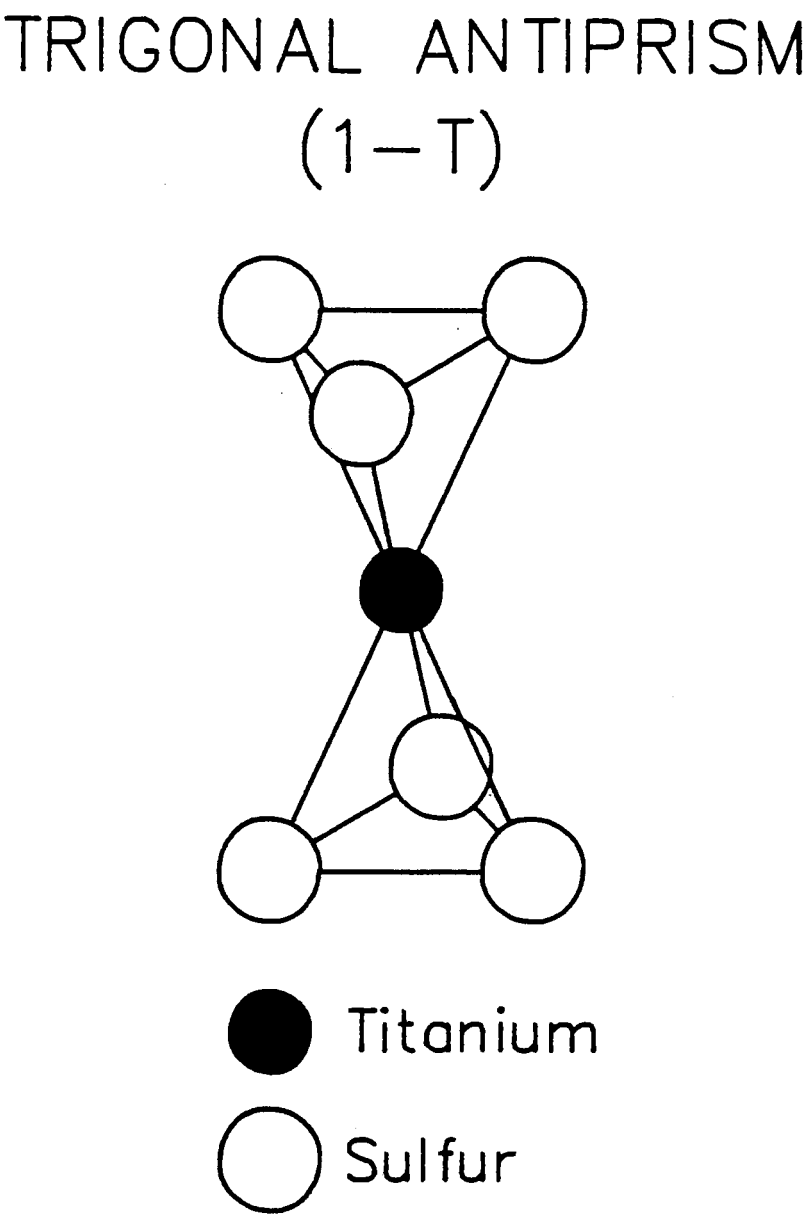

Figure 3

2-H coordination of chalcogen atoms with respect to the transition metal atom.

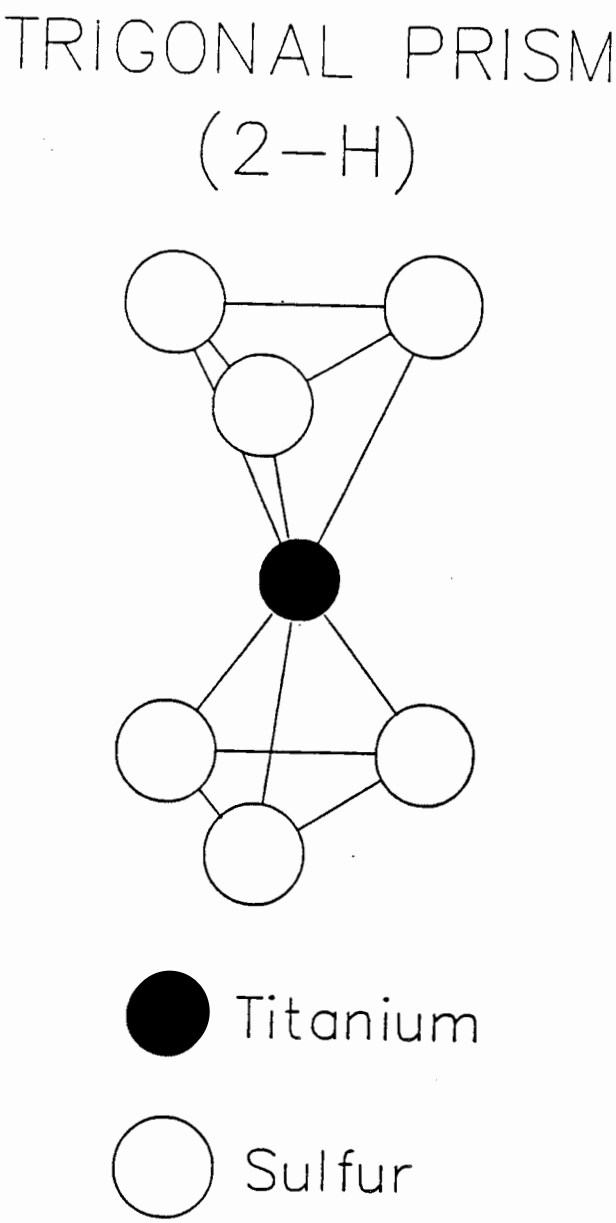

the structural, optical and electrical properties of the transition metal dichalcogenides has been documented by Wilson and Yoffe (30).

2-2 (a) Titanium Disulphide - Crystal Structure

Stoichiometric TiS_2 crystallizes in only one stable state forming a layered crystal having a golden metallic luster. It has the CdI_2 (trigonal antiprism) structure belonging to the space group C^4_{3v} with one formula unit per unit cell. TiS_2 is commonly referred to as $1T\text{-}TiS_2$ meaning a one layer stacking sequence with a trigonal primitive unit cell (Fig. 4). Each layer is made up of a hexagonal plane of titanium atoms sandwiched between two hexagonal planes of sulfur atoms. Chianelli et. al. (42) determined the atomic positions of the titanium and sulfur atoms within the unit cell to be:

Ti: 0 , 0 , 0

S : 1/3, 2/3, u 2/3, 1/3, -u

where $u \approx 1/4$. Thompson et. al. (57) found the lattice parameters of stoichiometric TiS_2 at room temperature to be:

$a = 3.4073 \pm 0.0002$ A

$c = 5.6953 \pm 0.0002$ A

Figure 4

TiS_2 atomic structure.

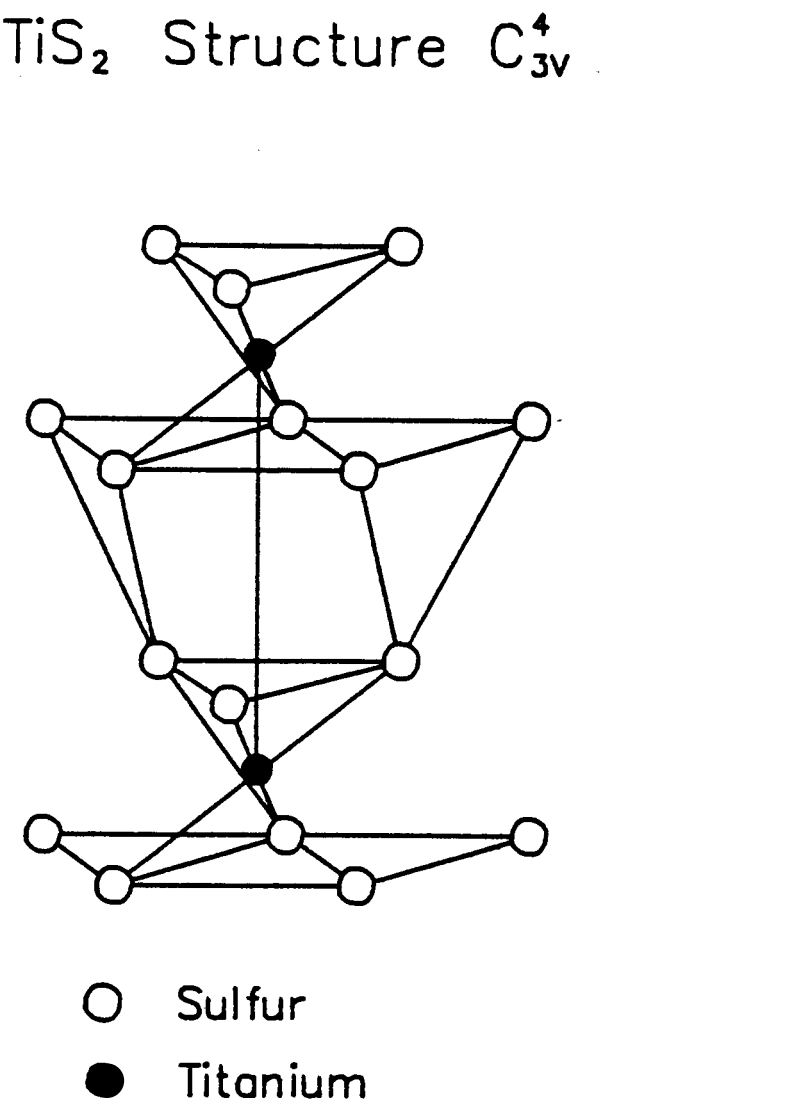

The TiS_2 sandwich layers are bound together by a weak Van der Waals type bonding, while the titanium and sulfur atoms making up each sandwich layer are predominantly covalently bonded. The relatively weak interlayer forces allow TiS_2 (like several other layered compounds) to accomodate extra atoms in this Van der Waals "region" (between the layers of TiS_2) without altering the original structure of the host layers. Symmetry and energy considerations indicate that there are two possible types of preferred sites within the Van der Waals "region" where the intercalated atoms are most likely to reside. The two types of sites are generally labelled "octahedral" and "tetrahedral" sites where the designations refer to the coordination of sulfur atoms around each site. There is one octahedral site and two tetrahedral sites for each TiS_2 unit. The larger octahedral sites (Fig. 5) are located midway between two TiS_2 layers directly above the Ti atoms (at the fractional coordinate 0, 0, 1/2), while the tetrahedral sites (Fig. 5) are located above the S atoms in planes just above and below the plane of octahedral sites within the Van der Waals layer (at the fractional coordinates 1/3, 2/3, z and 2/3, 1/3, -z where $z \approx 5/8$).

2-2 (b) Titanium Disulphide - Preparation

TiS_2 does not occur naturally but has been produced by at least four methods:

i) Heating titanium trisulfide to 600 C to disproportionate titanium trisulfide to form titanium disulfide and sulfur (38). The process is difficult to control however and usually results in substantial crystal imperfections.

ii) Reacting titanium tetrachloride with hydrogen sulfide to form titanium disulfide and hydrogen chloride (38), but substantial amounts of chlorine (up to 2 percent) have been found to contaminate the crystal.

iii) Reacting elemental titanium and sulfur directly at temperatures greater than 500 C to form titanium disulfide (38, 41), which can be well controlled for producing high quality powder samples.

iv) Chemical vapor transport techniques (41), which is the preferred method for growing high quality single crystals.

The TiS_2 powder used in the experiments for this thesis was prepared thermally in an elongated quartz ampoule using method iii). Stoichiometric amounts of titanium sponge (4 to 40 mesh) and elemental sulfur powder were placed in a well cleaned quartz tube (sealed at one end) under an atmosphere of dry argon. Particulate titanium sponge (4 to 40 mesh) was used instead of titanium wire or pellets because the sponge has a higher surface area to weight ratio which promotes higher reactivity and thus a faster, more complete reaction. Wittingham (33) states that using particulate titanium sizes smaller than 40 mesh resulted in uncontrollable reaction rates which causes localized heating resulting in crystal imperfections. The use of particulate sizes larger than 4 mesh resulted in unacceptably (or very) slow reaction rates.

A dry argon atmosphere was used when transferring the particulate titanium to the reaction tube in order to minimize contamination through the absorption of water vapor by titanium. The quartz tube containing the titanium and sulfur was then evacuated (to less than 10^{-4} torr) and sealed. The dimensions of the ampoule were 4.0 cm. in diameter by 40 cm. in length. The end of the ampoule containing the mixture of elemental titanium and sulfur was elevated by 5 cm. (Fig. 6) and placed in the two zone horizontal furnace. To physically separate the two constituents, the elevated end of the ampoule (containing

Figure 6

Thermal growth of TiS_2 powders.

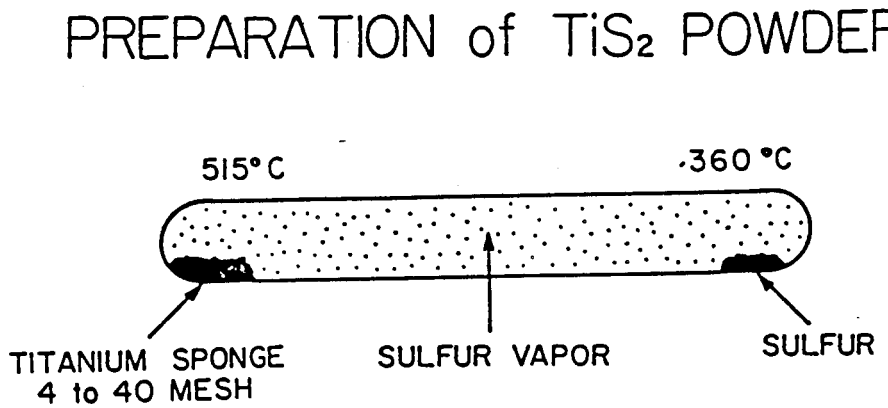

the titanium and sulfur mixture) was heated to 125 C while the opposite end of the ampoule was held at room temperature. The liquid sulfur (M.P. = 119 C) flowed to the cooler end of the ampoule carrying only a small fraction of the particulate titanium with it. The elemental titanium and sulfur were separated in order to control the vapor pressure of the sulfur surrounding the particulate titanium and thus control the reaction rate by varying the temperature of the licquid sulfur (38, 41).

The ampoule containing titanium sponge at one end and sulfur at the other end was then placed horizontally in a two zone furnace. The ampoule was differentially heated from 255 C and 100 C (titanium end and sulfur end respectively) to 515 C and 360 C at a rate of 1.75 C/hour in order to allow some time for heat dissipation from the exothermic reaction of the titanium and sulfur combining to form TiS_2. Mills (39) reports that temperatures of several thousand degrees may result when elemental titanium and sulfur are reacted directly. The ends of the ampoule were held at the high temperature limits (515 C and 360 C) for 48 hours in order to allow any remaining material to react. Finally the ampoule was removed from the furnace and shaken using an ultrasonic vibrator to break up any lumps of material and thoroughly mix the reacted product. The ampoule was again placed in an oven at 515 C for 48 hours to insure that all elements were completely reacted. The total mass of the sample contained

within the quartz ampoule was 70 grams.

The lattice parameters of the resulting powder were determined using X-ray diffraction patterns of the powders. The values of the lattice parameters (a = 3.406 ± 0.002 Å, c = 5.691 ± 0.004 Å) as determined from the X-ray data agree with the lattice parameters of stoichiometric TiS_2 reported by Thompson et. al. (57). The grain size of the powder was determined to be 5 - 15 um. in the basal plane by 1 - 3 um. thick using photographs of the powder taken with a scanning electron microscope.

2-2 (c) Titanium Disulphide - Stoichiometry

TiS_2 is usually a metal rich compound with the excess titanium atoms residing in the Van der Waals gap between the S-Ti-S layers. Winn et. al. (53) determined the chemical diffusion coefficients of sodium and lithium in $Na_xTi_yS_2$ and $Li_xTi_yS_2$ from electrochemical pulse experiments and found that the degree of intercalation of TiS_2 is highly dependent on the fraction of titanium residing in the Van der Waals gap. The titanium in the Van der Waals gap increases the interlayer interaction inhibiting the mobility of the intercalated species and possibly preventing the intercalation of some species (33, 47, 53).

Optical experiments (54, 55) indicate that TiS_2 is a semiconductor and calculations by Zunger et. al. (61)

indicate an indirect band gap of 0.2 - 0.3 ev. On the other hand temperature dependent resistivity measurements by Thompson et. al. (44) were interpretted to indicate that TiS_2 exibits semi-metallic properties. These conflicting observations can be reconciled (30) by assuming that TiS_2 is a "dirty semiconductor" meaning that even in stoichiometric TiS_2 some of the titanium atoms may be displaced from their usual locations and reside at vacant interlayer sites. Moret et. al. (62) modelled the effect of intersital titanium atoms to explain various anomalies in X-ray diffraction patterns of $Ti_{1+x}S_2$. Thompson et. al. (57) have found that the lattice parameters varied with the S/Ti ratio. They have measured the variation in the lattice parameters and the density as a function of the S/Ti ratio (for S/Ti in the range 1.80 - 2.00) and plotted the results (63), thus providing a direct method for determining the stoichiometry of TiS_2 samples from the lattice parameters.

2-3 (a) Intercalation of TiS_2 Powders

The insertion of guest atoms or molecules between the layers of a host (layered compound), without altering the atomic structure of the host lattice, is generally referred to as intercalation if the process is reversible. The guest species that has been successfully intercalated resides within the Van der Waals gap between the layers of the transition metal dichalcogenide compounds. Recent work (33)

has shown that Group Ib, Ia, IIb, IIa elements, aluminum, gallium, indium, thallium, as well as ammonia (or substituted ammonium compounds) can be intercalated into the transition metal dichalcogenides. The mechanism that drives the intercalation process is believed to be largely coulombic in nature (31). Whittingham (33, 34) has postulated that intercalation is a diffusion governed process and that in general, any species that is an electron donor could be intercalated into the layer compounds, and that there is some negative charge transfer from the intercalated species to the host layered compound. Kaluarachchi (32) used electron microscopy techniques to confirm that the guest species moves throughout the Van der Waals gaps of the host structure primarily by means of island motion. The movement of the Ag intercalation fronts in the Ag_xTiS_2 system was observed directly by optical methods and recorded on video tape.

Upon intercalation, the guest species does not usually fill all the Van der Waals regions uniformly but instead exibits a phenomenon called "staging". Staging refers to the guest species intercalating only selected Van der Waals regions in the host structure in an ordered sequence. The stage number "n" is the ratio of the number of successive Van der Waals regions divided by the number of regions containing the guest species, in an ordered sequence along the c-axis. For example, a "first stage" compound would have all successive Van der Waals regions occupied by the guest

species (Fig. 7) while an "n-stage" compound would have one of "n" successive interlayer regions of the host structure occupied by the guest species (Fig. 8, Fig 9). Fractional staging has been observed in KC_8 using elastic neutron-scattering (14), whereby a 3/2 stage compound would consist of 2 out of 3 successive Van der Waals regions being occupied by the intercalate species. Various attempts (58, 59, 60) have been made to explain the process of staging by considering the coulomb interactions between the intercalate species and strain effects in the host lattice. Two of the models which attempt to explain the process of staging are the Classical model of staging and the Island model of staging (32).

According to the Classical model of staging the Van der Waals regions in the host crystal are either uniformly occupied by the guest species or are completely empty (Fig. 7, Fig. 8, Fig. 9). In the classical model, the formation of higher stages from some initial stage compound involves either de-intercalation of the guest species with subsequent re-intercalation to form the higher stage compound or "tunnelling" of the guest species through the X-M-X host layers. The "de-intercalation, re-intercalation" process and the "tunneling" process both seem improbable in the formation of higher stages.

The island or "Daumas and Herold" model of staging has the guest species occupying all successive Van der Waals

regions. In this model the guest species does not occupy the layer uniformly but instead forms islands within the layer (Fig. 10). The periodicity of the islands along the c-axis of the crystal determines the stage of the compound. The higher stages may form simply by a re-arrangement of the islands of the intercalate species within the layers.

Only two distinct stages have been observed in the Ag_xTiS_2 system as opposed to up to ten distinct stages reported (40) in some of the intercalated graphite systems. The two stages reported (31) for Ag_xTiS_2 were stage 2 corresponding to x (x = mole fraction of silver intercalate) in the range x = 0.15 - 0.25 and stage 1 for x = 0.35 - 0.42 with mixed stage 1 and stage 2 co-existing for x = 0.25 - 0.35 (45). Scholtz and Frindt (31) have recently determined the structure of the stage 1 ($Ag_{0.4}TiS_2$) and stage 2 ($Ag_{0.2}TiS_2$) compounds using X-ray diffraction with a Debye Scherrer camera. The silver atoms were found to reside predominantly in the octahedral sites (31) of the interlayer region of the TiS_2 host crystal in both the stage 1 and stage 2 compounds. Scholtz (31) has plotted the variation in lattice parameters of Ag_xTiS_2 as a function of various values of x for both the stage 1 and stage 2 compounds, and thus the observed lattice parameters may be used as an indication of the degree of intercalation.

Figure 10

Daumas and Herold Island model of staging.

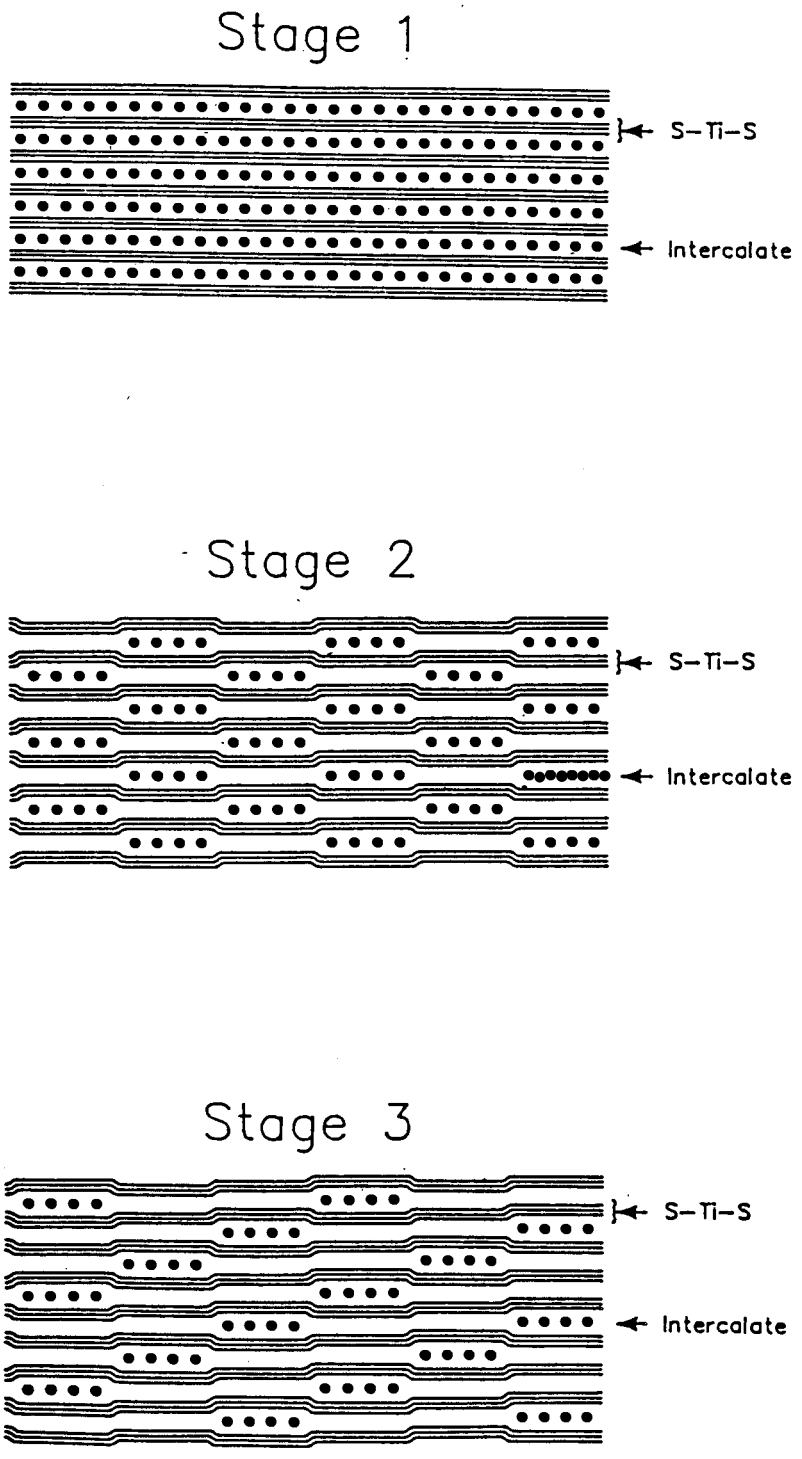

2-3 (b) Intercalation Methods

The process of intercalation is usually carried out by either electrochemical or thermal methods. Electrochemical intercalation of the dichalcogenides is usually accomplished by immersing a dichalcogenide cathode and an anode made up of the intercalate in a suitable electrolyte then electrically connecting the cathode and anode. The mole fraction of intercalate which enters the host dichalcogenide can be continuously monitored by coulombic measurements as the intercalation process proceeds. The mole fraction of intercalate may also be determined by comparing the weight of the dichalcogenide cathode before and after intercalation or by quantitative X-ray fluorescence techniques (32).

In the case of thermal intercalation, stoichiometric amounts of dichalcogenide powder and intercalate are placed inside evacuated ampoules and heated for some period of time. The intercalation of guest atoms generally causes an expansion in the host lattice perpendicular to the basal planes (typically 5 to 10 percent) and a less dramatic expansion parallel to the planes (typically 1 to 2 percent).

2-3 (c) Superlattice Formation

Another phenomenon exhibited by the guest intercalate species upon intercalation is the formation of superlattice structures by the guest species within the host structure.

There are two aspects to the formation of an intercalate superlattice:

i) intralayer ordering - the ordering of the guest species between the X-M-X layers of the host crystal (within an intercalate layer).

ii) stacking sequences - ordering of the intercalate layers with respect to other intercalate layers with the intercalate occupying different in plane sites in different layers (eg. intercalate occupying a, b, c sites in successive intercalate layers).

Parry et. al. (40) observed intralayer ordering in graphite layered compounds intercalated with potassium, rubidium and cesium. Culik and Chung (36) measured the temperatures and enthalpy changes of intralayer intercalate order-disorder transitions in Br_2 intercalated graphite using differential scanning calorimetric techniques. Evidence of the silver superlattice in Ag_xTiS_2 compounds has been observed indirectly by Suter (23) using X-rays and Leonelli (37) using Raman spectroscopy and directly by Unger et. al. (21) with electron diffraction.

The silver atoms intercalated in TiS_2 crystals were found to form an ordered triangular superlattice with a lattice parameter of $\sqrt{3}a_o$. The stacking sequence was assumed to be abc in accord with the findings of Scholz (31) and Leonelli (37). Subsequently the X-ray measurements of Suter et. al. (23) on $Ag_{0.33}TiS_2$ revealed the same $\sqrt{3}a_o$ x $\sqrt{3}a_o$ intralayer ordering with an abab... stacking sequence.

2-4 Sample Preparation and Specifications

Ag_xTiS_2 samples were prepared thermally by heating the appropriate amounts of silver powder and TiS_2 powder in an evacuated quartz ampoule. The silver powder was obtained from Materials Research Corporation and the TiS_2 powder was prepared as specified in section 2-2. Samples of Ag_xTiS_2 in the range $0 < x < 0.7$ were prepared by mixing appropriate weight quantities of the silver and TiS_2 powders (total weight for each sample = 0.5 gm.).

The mixture was placed in quartz ampoules (typically 1 cm. O.D x 7-12 cm. long) and evacuated ($< 10^{-4}$ torr) while heating the ampoule (to 150 C) with heating tape to remove excess oxygen adsorbed on the walls of the ampoule (in order to prevent the possible formation of TiO_2). The sealed ampoules were then shaken using an assortment of vibrators to obtain a homogeneous mixture of silver and TiS_2 powder in the ampoule.

Two groups of samples were prepared and labelled group A and group B. The ampoules were then uniformly heated to 800 C and 1000 C (for group A and group B samples respectively) for a period of 4 - 8 days. The samples were cooled once during the 4 - 8 day intercalation period to room temperature and shaken vigorously in an attempt to break up any lumps of material and obtain a uniform mixture of any unreacted constituents then placed back into the oven for the remaining 4 - 8 day intercalation period.

The final step in the preparation of the intercalated samples was to drop quench the ampoules (from 800 C - group A and 1000 C - group B) by dropping them into a beaker of cold tap water. The samples were then screened using a stainless steel screen having 200 um. holes to separate any remaining lumps of material before being tested.

The resulting powders were in the form of hexagonal platelets having a typical size in the range of 5 - 15 um. x 1 - 3 um. thick as determined from pictures taken using a scanning electron microscope. X-ray Fluorescence and X-ray data were then taken to verify the integrity and composition of the samples.

CHAPTER 3

Sample Characterization

3-1 (a) XRF Sample Verification

(GROUP A - quenched from 800 C)

X-ray fluorescence (XRF) spectra were obtained from of the Ag_xTiS_2 powder samples which were quench cooled from 800 C (group A) as a check of the ratio of Ag to TiS_2. A SIEMENS KRISTALLOFLEX 2 X-ray generator was used to generate Zn K_a (8.631 Kev.) and Zn K_b (9.572 Kev.) X-rays. The energies of the emitted X-rays are characteristic of the element.

The various (group A) powder samples ($0 < x < 0.6$) were placed on a polyester film (< 4 um. thick) over the incident Zn X-rays. A KEVEX-RAY 0800 Si(Li) detector located 2 cm. from the sample perpendicular to the incident X-rays was used to detect the intensities of the fluorescent X-rays emitted from the sample. The data was collected using a NUCLEAR DATA ND-66 multi-channel analyzer with windows set up around the sulfur K_a, titanium K_a, and silver L_a peaks. The intensities of the respective peaks are directly related to the weight concentration of the element in the sample.

Intensity ratios of S/Ti and Ag/Ti were calculated from the intensity measurements and plotted as a function of the mole fraction of silver (x) as determined from weight measurements (Fig. 11). The intensity ratio of S/Ti was

Figure 11

Verification of the Ag/Ti ratio for group A (quenched from 800 C) samples using X-ray flourescence. Integrated intensity of the silver L_a peak divided by the integrated intensity of the titanium K_a peak versus the mole fraction of silver (x) in Ag_xTiS_2 as determined by weighing.

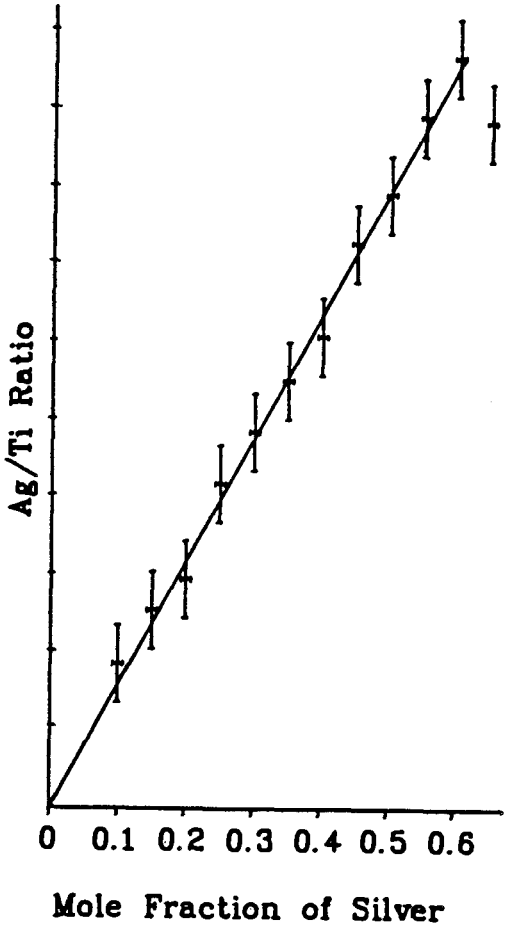

calculated in order to determine the accuracy of the method (since the S/Ti ratio should remain constant for all samples). The accuracy of the latter method for determining the relative amount of a particular element was determined to be ±15% from the S/Ti ratio. The XRF results agree (to within 15%) with the mole fraction of silver (X) determined by weighing for $0 < X < 0.5$, and provides verification of the ratio of Ag to TiS_2 in the Ag_xTiS_2 samples.

3-1 (b) XRF Sample Verification

(GROUP B - quenched from 1000 C)

X-ray fluorescence (XRF) spectra were taken of the group B (quenched from 1000 C) Ag_xTiS_2 powder samples as a check of the ratio of Ag to TiS_2. The samples were mounted on graphite blocks and an ISI-DS130 scanning electron microscope equiped with an Ortec EG+G EEDS II X-ray energy detector and analysis system was used to analyze the composition of the Ag_xTiS_2 powders. The sample was bombarded by energetic electrons which excite the atoms contained within some volume of the sample material. The stock TiS_2 powder was used as the reference with the S/Ti ratio assumed to be exactly 2.0 in order to calibrate the equipment. The intensities of the sulfur K_a (2.308 KeV), silver L_a (2.984 KeV) and titanium K_a (4.510 KeV) lines were measured using a 15 KeV electron beam to excite the sample and ratios of S/Ti and Ag/Ti calculated for each of the (group B) Ag_xTiS_2 samples. The penetration

depth of the beam was estimated to be 1.5 um. from earlier determinations of the penetration depth in Ag_xTiS_2 single crystals using 10 kV and 20 kV electron beams by Kaluarachchi (32). The results of the XRF results for sample B (quenched from 1000 C) are shown in Fig. 12. The ratio of Ag/Ti determined from the XRF analysis agree within experimental error in each case with the ratio of Ag/Ti determined from the weights of Ag and TiS_2 powders that were initially mixed together in the quartz ampoules prior to intercalation.

3-2 (a) X-ray Diffraction - GENERAL PROCEDURE (DATA)

X-ray diffraction data were taken for all samples using a Philips PW 1730 X-ray generator with a copper anode and nickel filter (to isolate the copper K_a radiation) and equipped with a PW 1050/25 diffractometer. The data were collected using a Camberra Nuclear Counter (model 1775) and an IMS 8000 computer. The resulting copper K_a and K_b peaks were used to determine the lattice parameters of the samples. The data were collected over the 2 theta angular range of 10 to 140 degrees in steps of 0.05 degrees with count times of 2 to 40 seconds at each step. The equipment was calibrated using pure silver powder. In addition, many of the sample scans contained very weak TiO_2 diffraction peaks (from small amounts of TiO_2 present in many of the samples). The TiO_2 lines were used to check the calibration of the equipment when they were present.

Figure 12

Verification of the Ag/Ti ratio for group A (quenched from 1000 C) samples using X-ray flourescence. Integrated intensity of the silver L_a peak divided by the integrated intensity of the titanium K_a peak versus the mole fraction of silver (x) in Ag_xTiS_2 as determined by weighing.

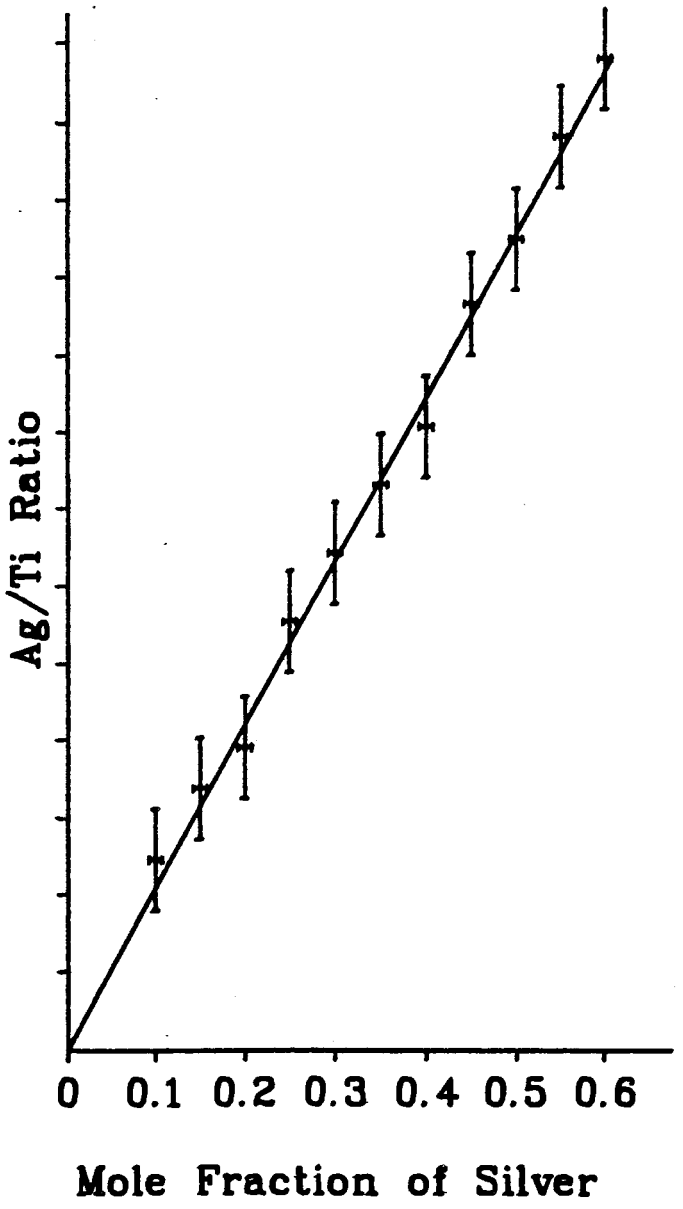

3-2 (b) X-RAY - Lattice Parameter Determination

The lattice parameters of the various samples were determined using the following algorithm:

1) The X-ray diffraction patterns were first indexed (Miller indices h k l identified) for a few of the easily identified peaks (eg. 001, 101, 102, 110, 111, etc...)

2) Lattice parameters were calculated on the basis of the indexed peaks using the equations 3-1 and 3-2 with a two parameter fitting program:

$$2 * d * \sin(\theta) = n * w \quad \text{- diffraction equation} \qquad 3\text{-}1$$

$$\sin(\theta) = (h^2+h*k+k^2)/(3*a^2) + l^2/(2 * c)^2 \qquad 3\text{-}2$$

where: d = spacing between planes of atoms corresponding the Miller indices h k l.

w = wavelength of the X-rays

n = order number of the diffraction peak

a, c = lattice parameters of the hexagonal unit cell.

θ = angle between the incident X-rays and the sample.

3) Peak positions of K_a and K_b lines were then calculated based on the previously calculated lattice parameters.

4) The calculated peak positions were compared to the data facilitating the indexing of additional peaks.

5) If a significant number non-indexed lines remain then return to step 2).

Fig. 13 shows the indexing of X-ray diffraction patterns for the pure TiS_2 (x = 0), stage 2 Ag_xTiS_2 (x = .20) and stage 1 Ag_xTiS_2 (x = .40) samples.

3-3 (a) X-RAY - Lattice Parameters of the TiS_2 Stock Powder

X-ray diffraction data were first taken of the TiS_2 stock material to verify the quality. The lattice parameters of the starting TiS_2 powder were determined by indexing 37 of the copper K_a and K_b diffraction lines using the algorithm of 3-2(b). No evidence of pure sulfur, titanium or TiO_2 was found. The lattice parameters of the stock TiS_2 were calculated from the X-ray data to be a = 3.406 $\pm$ 0.002 Å and

Figure 13

Indexing of X-ray diffraction patterns

for x = 0.40, x = 0.20, and x = 0.

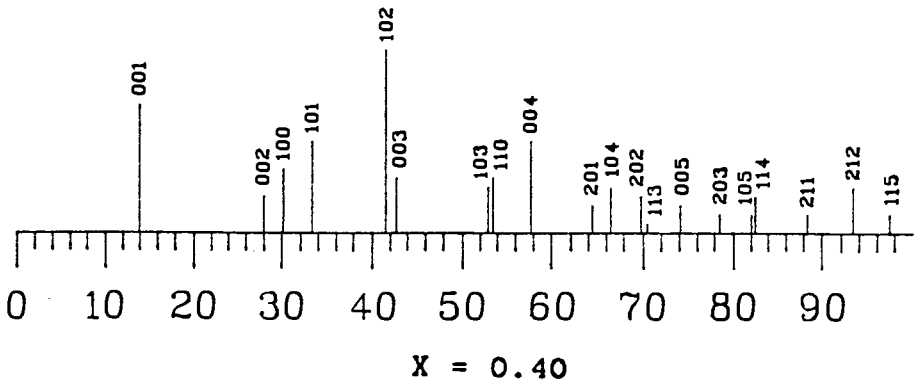

X = 0.40

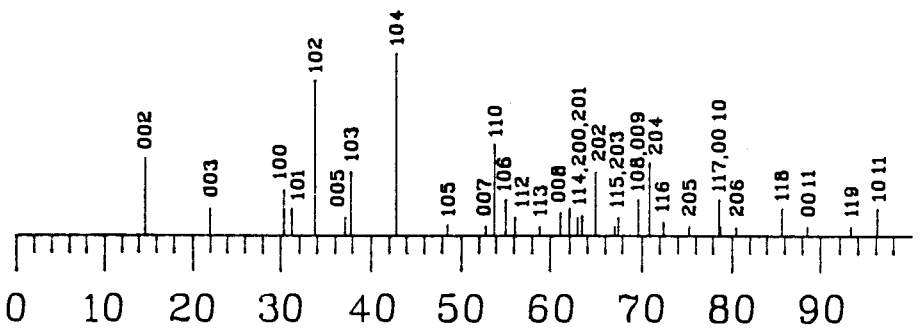

X = 0.20

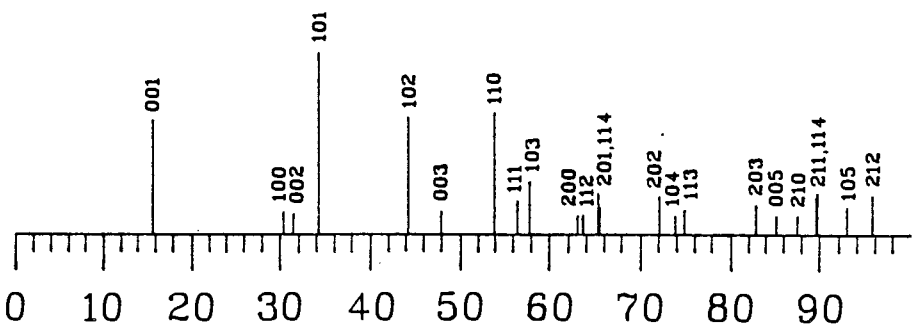

X = 0

c = 5.691 ± 0.004 A in agreement with previously determined and accepted values (57, 30, 63). The graph of S/Ti ratio vs lattice parameters compiled by Jacques et. al. (63) was used to verify that the ratio of S/Ti = 2.00 ± 0.02 for the TiS_2 powder used in this work.

3-3 (b) X-ray - Lattice Parameters

Group A (quenched from 800 C)

X-ray data was taken at room temperature of the group A samples. The diffraction peaks were identified and the lattice parameters calculated using the algorithm outlined in 3-2 (b). The lattice parameters of the pure TiS_2 were found to expand linearly with increasing values of x = 0 to $x \leq 0.15$, supporting the interpretation by Scholtz et. al. (31) and Gerards et. al. (65) that the silver atoms behave like a dilute gas which initially uniformly populate the Van der Waals gaps in the host TiS_2 crystal. The lattice parameters were plotted as a function of silver mole fraction in Fig. 14a and Fig. 14b.

The lattice parameters of the samples where $0.15 < x < 0.30$ were identified from the position of the diffraction lines to be pure stage 2 samples. Silver mole fractions in the range $0.3 < x < 0.5$ were predominantly stage 2 with small amounts of stage 1 present. Figures 14a and 14b represent a graphical summary of the X-ray diffraction results of the Group A samples (quenched from 800 C). Pure

Figure 14a

Hexagonal lattice parameter a (Å) versus silver mole fraction x for the group A samples.

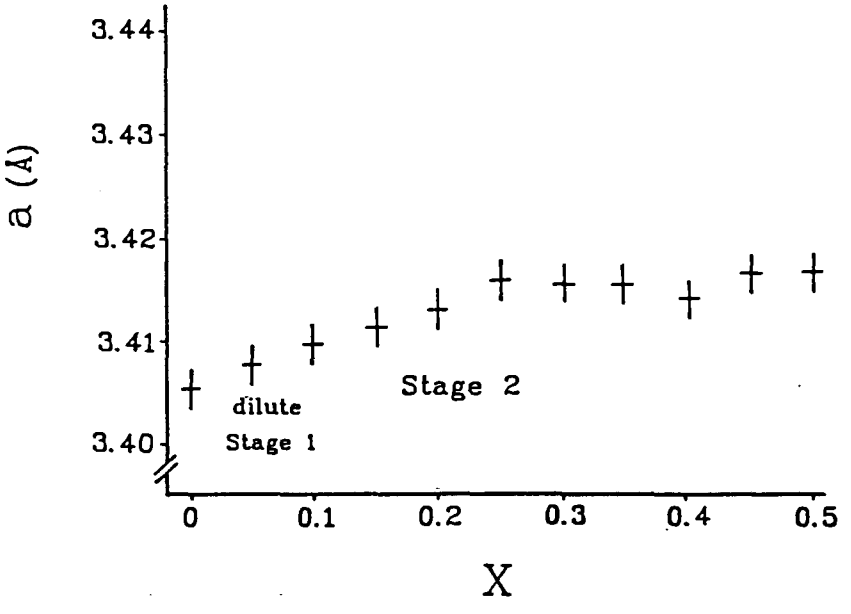

Figure 14b

Hexagonal lattice parameter c (Å) versus silver mole fraction x for the group A samples.

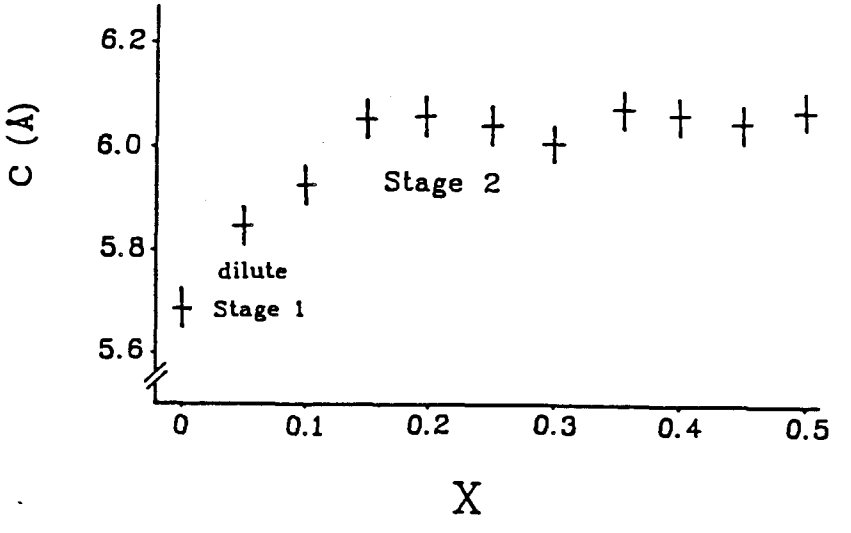

silver diffraction lines were present for all samples with $x > 0.5$ meaning that the high concentration samples ($x > 0.5$) were not completely intercalated, and that crystalline silver was present in addition to Ag_xTiS_2. The samples with $x > 0.5$ were eliminated from all future work on the basis of the X-ray data. There was no evidence of pure silver diffraction lines for $Ag_{0.5}TiS_2$ in contrast with results obtained by Scholtz et. al. (45) who reported that the maximum mole fraction of silver that could be intercalated electrochemically or thermally was x 0.42. The group A samples (cooled from 800 C) agree with the results obtained by Scholz et. al. (63) and Gerards et. al. (65) only for values of $0 < x < 0.25$. The higher silver concentration samples ($x > 0.25$) prepared for this work at 800 C are predominantly stage 2 in contrast with the predominantly stage 1 structures reported by Scholtz et. al. (63) and Gerards et. al. (65).

3-3 (c) X-RAY Lattice Parameters - Group B (quenched 1000 C)

Room temperature X-ray data were obtained for each of the group B (quenched from 1000 C) samples. The peaks were identified and lattice parameters calculated using the algorithm in 3-2 (b). Fig. 15a and Fig. 15b are a summary of the lattice parameters vs. silver mole fraction as determined from the data. The X-ray diffraction patterns of the Ag_xTiS_2 samples which were quench cooled from 1000 C clearly show

Figure 15a

Hexagonal lattice parameter a (A) versus silver mole fraction x for the group B samples.

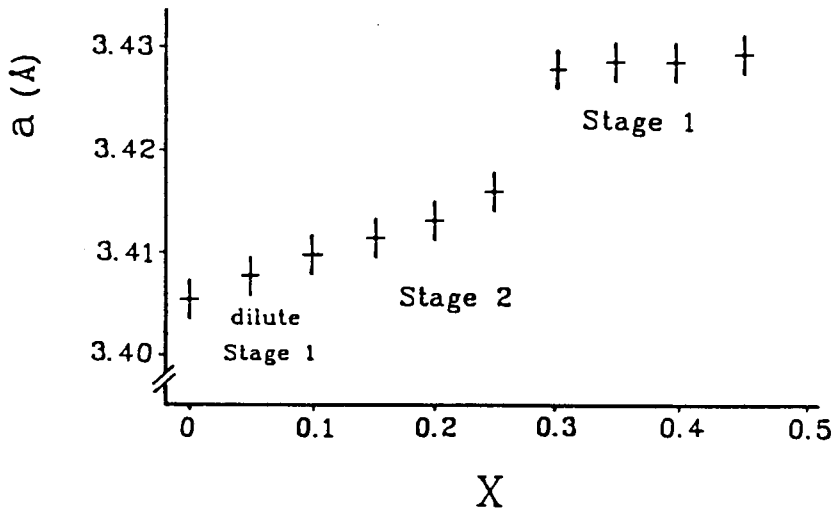

Figure 15b

Hexagonal lattice parameter c (A) versus silver mole fraction x for the group B samples.

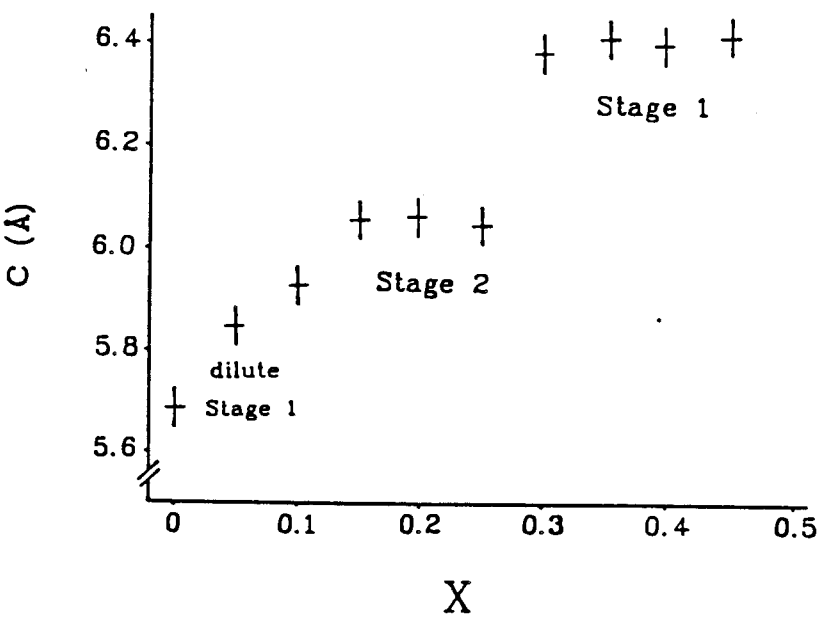

that the Ag_xTiS_2 is pure stage 2 for $0.15 < x < 0.25$ with mixed stage 1 and stage 2 for $0.25 < x < 0.35$ and pure stage 1 for $x > 0.35$. The c-axis lattice parameter was found to increase uniformly from $\simeq 5.7$ Å (pure TiS_2) to $\simeq 6.0$ Å as a function of the mole fraction x (for $0 < x < 0.15$) then increase to 12.1 Å for the stage 2 compound ($0.15 < x < 0.25$) which to a first approximation may be seen as consisting of an un-intercalated layer having a spacing of $\simeq 5.7$ Å and an intercalated layer having a spacing of $\simeq 6.4$ Å assuming that the empty TiS_2 layer retains the same spacing as pure TiS_2 in the stage 2 structure. For $0.25 < x < 0.35$ there was a co-existance of stage 1 having a c parameter $\simeq 6.4$ Å and stage 2 with c $\simeq 12.1$ Å. The c parameter for $x > 0.35$ was $\simeq 6.4$ Å for the stage 1 compound. However there was some evidence of conversion to stage 2 compounds over a period < 6 months for samples with $x > 0.30$ indicating that stage 1 compounds are somewhat unstable at room temperature and that the mole fraction limits ($0.25 < x < 0.35$) of the stage 1 - stage 2 region may be a function of the cooling rate in preparing the thermally intercalated samples. It appears that the maximum average separation of TiS_2 layers is $\simeq 6.0$ Å and that the intercalation of silver for $x > 0.35$ increases the free energy of the crystal causing the pure stage 1 intercalation phase to be unstable at room temperature and eventually decay (and possibly de-intercalate) to the more stable stage 2 structure ($0.15 < x < 0.25$). A summary of the stage and

lattice parameters vs silver atom concentration is shown in Fig. 15a and Fig. 15b. The x-ray diffraction results from the thermally intercalated samples which were quench cooled from 1000 C agree very well with results obtained from the electro-intercalated and thermally intercalated samples used by Scholtz (31) and Gerards et. al. (65).

3-4 X-RAYS GROUP C (annealed from 1000 C - group 2)

A new group of Ag_xTiS_2 samples (group C) $0 < x \leq 0.5$ was prepared in order to investigate the differences in the X-ray diffraction patterns between the Ag_xTiX_2 samples which were quench cooled from 800 C (forming predominantly stage 2 compounds) and samples quench cooled from 1000 C (forming both stage 1 and stage 2 compounds). The group C samples were prepared using the same procedure as the previous two groups except that they were intercalated at 1000 C and cooled over a period of 10 hours instead of being quench cooled.

X-ray and XRF analysis was then done on each of the slowly cooled (Group C) Ag_xTiS_2 samples. The X-ray diffraction patterns for these samples were similar to the patterns from the pure TiS_2 having lattice parameters a = 3.406 to 3.408 ± 0.002 Å and c = 5.690 to 5.708 ± 0.004 Å for $0 < x \leq 0.5$. There were also weak TiO_2 X-ray diffraction lines present which were used as a calibration check on the equipment but suprisingly no pure silver lines appeared in

the diffraction patterns. There was little or no evidence of intercalation as determined from the X-ray data on the group C samples. The XRF analysis of the samples resulted in inconsistantly high and low values for the ratios of Ag/Ti which varied over different portions of the sample. Based on the X-ray diffraction and XRF results, the Ag + TiS_2 samples which were cooled slowly from 1000 C were not intercalated to any significant degree. It is possible that the silver was distributed over the surface of the TiS_2 crystalline powder in such a way that very little or no crystalline silver was present which is supported by the absence of pure silver X-ray diffraction lines.

CHAPTER 4

DIFFERENTIAL SCANNING CALORIMETRY

4-1 General Discussion

Differential scanning calorimetry (DSC) is a technique whereby a sample material and a reference material are heated or cooled while a quantity which is proportional to the differential enthalpic change (or change in heat capacity) between the sample and reference materials is measured. The data are recorded as a function of time or temperature. Enthalpic changes are caused by fundamental changes in state, chemical composition, molecular reactivity of the materials, etc. The shape of the enthalpy change vs temperature or time is basically a function of the reaction kinetics but is also influenced by sample packing, geometric shape of the sample and reference, the heating rate, atmosphere, temperatures of the sample and reference, thermal contacts at all interfaces, as well as the time constants of the electronics, etc. The sample and reference materials are placed in identical containers which may or may not be hermetically sealed, then placed in thermal contact with a heat source. A uniform linear rate of heating is usually desired because of the time dependence of the measured quantity. Thermocouples are used to monitor the temperatures of the sample and reference.

4-2 Two Standard Methods of DSC

Two different approaches have been used to determine the difference in enthalpic changes between a sample and reference material with respect to time or temperature. One approach (used by the Perkin-Elmer Company) was to apply differential heating to the sample and reference in order to maintain a constant temperature difference between the sample and reference material. The difference in power supplied to each heater is related to the difference in enthalpic changes between the sample and reference. The second approach (used by the Dupont Company) was to apply heat to the sample and reference at a uniform rate while measuring the temperature difference of identical chromel wafers (of known mass m and specific heat C - Fig. 16) situated close to the sample and reference and thus indirectly measuring the difference in heat flow ($dq_r/dt - dq_s/dt$) between the sample and reference where $dq/dt = m*C*dT/dt$ for the sample and reference respectively.

4-3 Theory of Operation

The two approaches to DSC may be better understood through an understanding of a simplified theoretical treatment of the basic principles of differential scanning calorimetry. The DSC cell is shown in Fig. 16. The principles of DSC are derived from the rearrangement of the

Figure 16

DSC sample chamber.

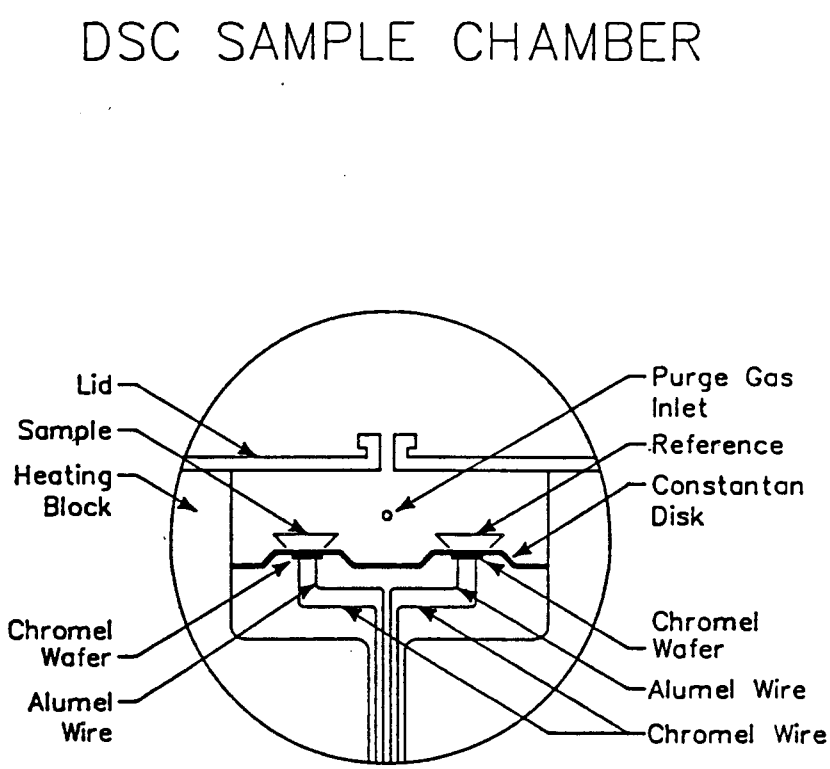

following two equations, which apply to the simplified model (Fig. 17) of the DSC apparatus used in the experiments described later.

Conservation of energy $$dh/dt = C_S * dT_S/dt - dq_S/dt \quad (4-1)$$

Newton's law $$dq_S/dt = (T_p - T_S)/R \quad (4-2)$$

where:

dh/dt - is the rate at which the sample generates energy.

C_S - is the specific heat of the sample.

dT_S/dt - is the rate of temperature increase of the sample.

$C_S * dT_S/dt$ - is the rate that energy is being used to increase the temperature of the sample.

dq_S/dt - is the rate of energy flow from/to the sample through the thermal resistance R.

T_p - is the temperature of the heat source/sink.

T_S - is the temperature of the sample.

R - is the thermal resistance between the

Figure 17

Simplified model of the DSC sample chamber.

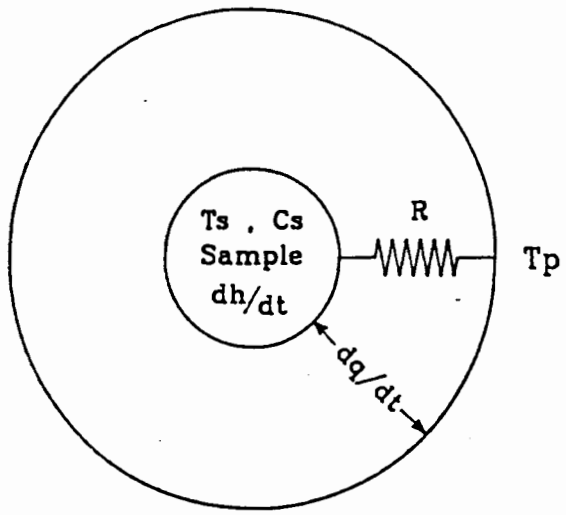

R – thermal resistance
Ts – sample temperature
Tp – thermal energy source/sink
Cs – specific heat of sample
dh/dt – energy generated/absorbed by the sample
dq/dt – rate of energy flow to/from the sample

sample/source and the heat source/sink, and between the reference/source and the heat source/sink.

(All energy exchanges occur through the thermal resistance R).

Equations 4-1) and 4-2) written for the sample (subscript s) and the reference (subscript r) are:

$$dh/dt = C_S * dT_S/dt - dq_S/dt \quad \text{sample} \quad 4\text{-}3a$$

$$0 = C_r * dT_r/dt - dq_r/dt \quad \text{reference} \quad 4\text{-}3b$$

$$dq_S/dt = (T_p - T_S)/R \quad \text{sample} \quad 4\text{-}4a$$

$$dq_r/dt = (T_p - T_r)/R \quad \text{reference} \quad 4\text{-}4b$$

Combining equations 4-(3a) and 4-(3b) for the sample and the reference:

$$dh/dt = (C_S - C_r) * dT_r/dt + C_S * d/dt(T_S - T_r) - d/dt(q_S - q_r) \quad 4\text{-}5$$

Combining equations 4-4a and 4-4b for the sample and reference:

$$d/dt(q_S-q_r) = -(T_S-T_r)/R \qquad 4\text{-}6$$

and differentiating equation 4-6 yields

$$d^2/dt^2(q_S-q_r) = -(T_S-T_r)/R \qquad 4\text{-}7$$

Substitution of equation 4-7 into equation 4-5 gives

$$dh/dt = (C_S-C_r)*dT_r/dt - R*C_S*d^2/dt^2(q_S-q_r) - d/dt(q_S-q_r) \qquad 4\text{-}8$$

A rearrangement of equation 4-8 yields

$$d/dt(q_S-q_r) = (C_S-C_r)*dT_r/dt - R*C_S*d^2/dt^2(q_S-q_r) - dh/dt \qquad 4\text{-}9$$

It is assumed that the reference material generates no energy (undergoes no phase transistions) and thus $dh_r/dt = 0$. Thus for a constant heating rate (dT_p/dt) the rate of energy flow to or from the reference is constant (dq_r/dt = constant) and therefore $d^2q_r/dt^2 = 0$ and $dT_p/dt = dT_r/dt$.

Re-writing equation 4-9 with the latter restriction:

$$d/dt(q_S - q_r) = (C_S - C_r)*dT_p/dt - R*C_S*d^2q_S/dt^2 - dh/dt \qquad 4\text{-}10$$

$(C_S - C_r)$ - specific heat difference between the sample and reference material.

dT_p/dt - rate of change of the temperature of the heat source/sink.

$R*C_S$ - is a thermal time constant which is a measure of the thermal response of the sample.

dq_S/dt - rate of change of heat flow between the sample and the surroundings through the thermal resistance R.

dh/dt - rate that energy is generated by the sample while the sample is undergoing a transition.

4-4 Typical DSC Curves

A typical DSC curve is shown in Fig. 18. Positive excursions from the baseline indicate exothermic transitions in the case of DUPONT DSC scans and endothermic transitions in the case of PERKIN-ELMER DSC scans. During the first section of the curve (Fig. 18), the sample undergoes no

Figure 18

Typical DSC curve during heating.

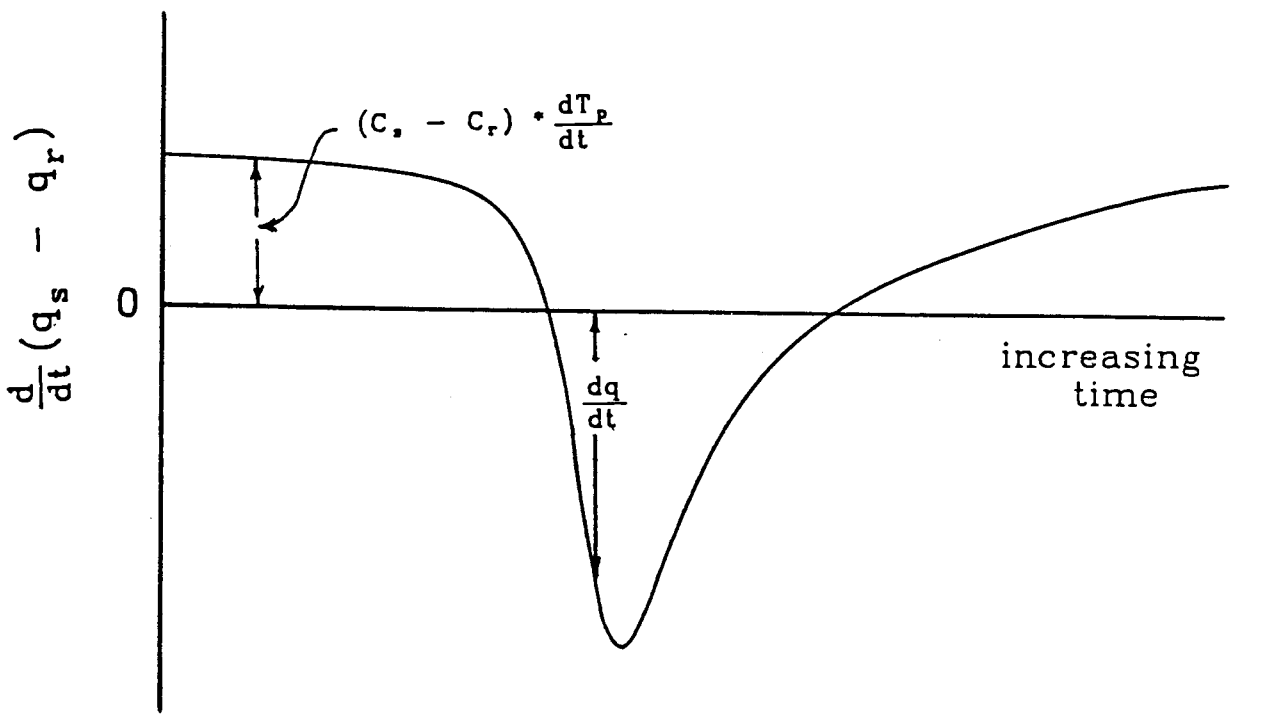

transitions ($dh/dt = 0$, $T_S - T_r$ = constant, $d/dt(q_S - q_r)$ = constant) so that the baseline displacement from zero is due solely to mismatches in the specific heats of the sample and reference ($C_S - C_r$) multiplied by the heating rate dT_p/dt. During a transition the height of the curve as measured from the baseline is a measure of the rate of the transition kinetics (the rate that the sample generates or gives off heat energy during the transition = dh/dt) in the case of first order transitions. The slope of the transition part of the curve is a measure of a thermal time constant ($R*C_S$) for the equipment used multiplied by the difference in the rate that differential energy is being applied to the sample and reference $d^2/dt^2(q_S - q_r)$ in the case of PERKIN-ELMER equipment. Similarly in the case of Dupont equipment the slope of the transition part of the curve is a measure of a thermal time constant ($R*C_S$) multiplied by the rate that the temperatures between the sample and reference are changing divided by the thermal resistance ($1/R * d/dt(T_S - T_r)$).

4-5 Modifications

The Dupont Series 99 Thermal Analyzer was used to control a Dupont Differential Scanning Calorimeter (DSC) cell base with a modified standard DSC cell and modified liquid nitrogen cooling accessory. The specified operating temperature range of the DSC cell is between -180 C and 725 C when equipped with the optional liquid nitrogen cooling

accessory supplied by Dupont. The liquid nitrogen cooling accessory was found to be inadequate for extended operation below ambient temperature due to the rapid boiloff of the liquid nitrogen. Refilling during a run disrupted the stability of the equipment and disturbed the measurements. The small liquid nitrogen volume (50 - 75 cc.) that the cooling accessory was designed for would completely evaporate in less than 10 min. while the time required to cool the apparatus to temperaturtes below -100 C is greater than 10 min. A larger dewar (Fig. 19) coupled to a copper block using a glass-to-metal seal was built to expand the liquid nitrogen capacity of the Dupont cooling accessory. The dewar was built to hold approximately one litre of liquid nitrogen which would last 45 - 90 minutes depending on the type of operation (cooling/heating) and temperature ranges of the scans. The top of the dewar had a styrofoam lid to slow down the evaporation of the liquid nitrogen.

The design of the cooling apparatus is such that the outside surfaces of the cooling accessory and DSC cell are exposed to the atmosphere resulting in the condensation of water vapor. Subsequent operation from -40 C to 20 C causes water to accumulate at the outside base of the DSC cell. The base of the DSC cell is not water proof (as manufactured) and the electrical and thermal insulation inside the cell absorbs the condensed water at the base of the cell ultimately shorting the heater wire connections within the cell and

Figure 19

Differential Scanning calorimeter cell.

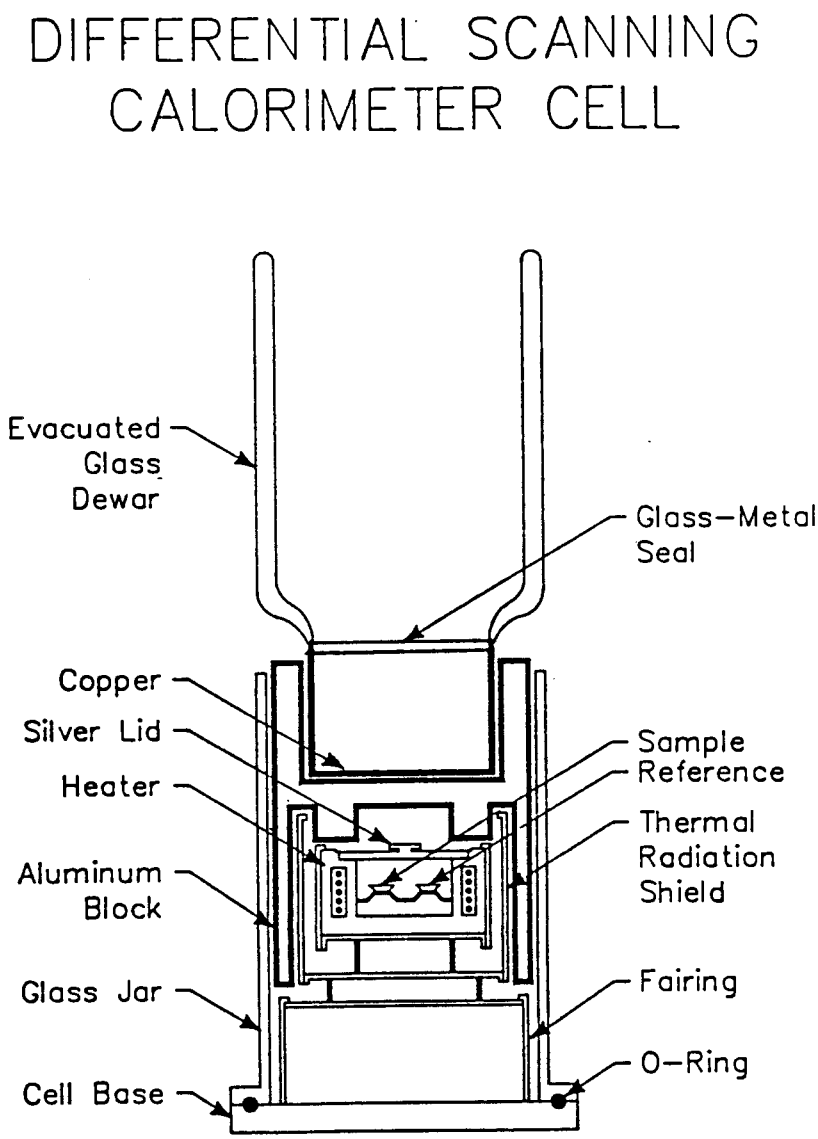

destroying many of the electronic circuits within the DSC controller. The DSC cell was partially dismantled and completely sealed with a silicone compound around the outer stainless steel shell of the DSC cell. This protected the inner part of the cell from the water which accumulated around the outer base. A plastic sleeve also was fitted over the dewar and DSC cell in order to prevent condensation of water vapor from the room. A dry nitrogen purge of the cell and dewar was also used to remove water vapor from inside the plastic sleeve.

4-6 Temperature Calibration

The indium samples provided with the calorimeter were used as calibration standards. Indium sample weights of 1.59, 3.50, 7.26 and 19.82 mg. were hermetically sealed in the aluminum sample pans. Each of the indium samples was run in the DSC cell using an empty sample pan + lid as the reference material. The programmed heating rate was 10 K/min. Different sizes of calibration sample were used in order to determine the dependence of the measured transition temperature on the sample size. The transition temperature as determined from the data was within ± 0.5 K of the melting point of indium (429.6 K) for all of the indium samples used. There was no indication of dependence of the transition temperature on sample size although the transition peak was slightly broader for the larger samples.

The temperature calibration of the DSC equipment was then checked by using a variety of different powders and crystals in order to evaluate the accuracy of measured melting transition temperatures especially when powders and small crystals were used as the sample. The following substances were used:.

Substance	Transition Temperature	Form
AZOBENZOL	341 K	red crystals
BENZIL	368 K	yellow crystals
ACETANILID	388 K	white crystals
PHENACETIN	408 K	white crystals
BENZANILID	436 K	white powder
SALOPHEN	464 K	white powder
DICYANDIAMID	483 K	white powder
SACCHARIN	501 K	white crystals

In all cases, the recorded transition temperature were within ±1 K of the stated transition temperature.

The melting points of gallium and mercury were used to check the calibration temperature at lower temperatures. Small samples of gallium and mercury were frozen using liquid nitrogen and hermetically sealed in aluminum sample pans at temperatures below their respective melting points. The

measured melting points of the mercury (M.P. = 234.6 K) and gallium (M.P. = 302.8 K) were within 0.5 K of the accepted values when heated at 10 K/min.

Different heating rates were used with the 3.50 mg. indium sample and empty reference pans in order to determine the dependence of the recorded transition temperature on heating rate (Fig. 20). Heating rates of 1, 2, 5, 10, and 20 K/min. were used. The average increase in the recorded transition temperature was 0.3 K for each factor of 2 increase in the heating rate for heating rates above 2 K/min. The recorded transition temperature was the same for heating rates of 1 and 2 K/min.

Cooling rates of 1, 2, 5, and 10 K/min. were obtainable with the 3.50 mg. indium sample. The average decrease in the measured transition temperature was less than 0.2 K for each factor of 2 decrease in the cooling rate. The difference between the transition temperatures measured for heating and cooling decreased as the heating/cooling rate decreased as expected. Heating or cooling the sample at slower rates reduces the possibility of superheating or supercooling the sample before the sample undergoes any first order transitions. An effect of using low heating/cooling rates is that the recorded transition peak becomes lower and broader thus making it difficult to accurately determine the starting point of the transition and thus the transition temperature.

Figure 20

dh/dt vs. TEMPERATURE
for different
SCAN RATES

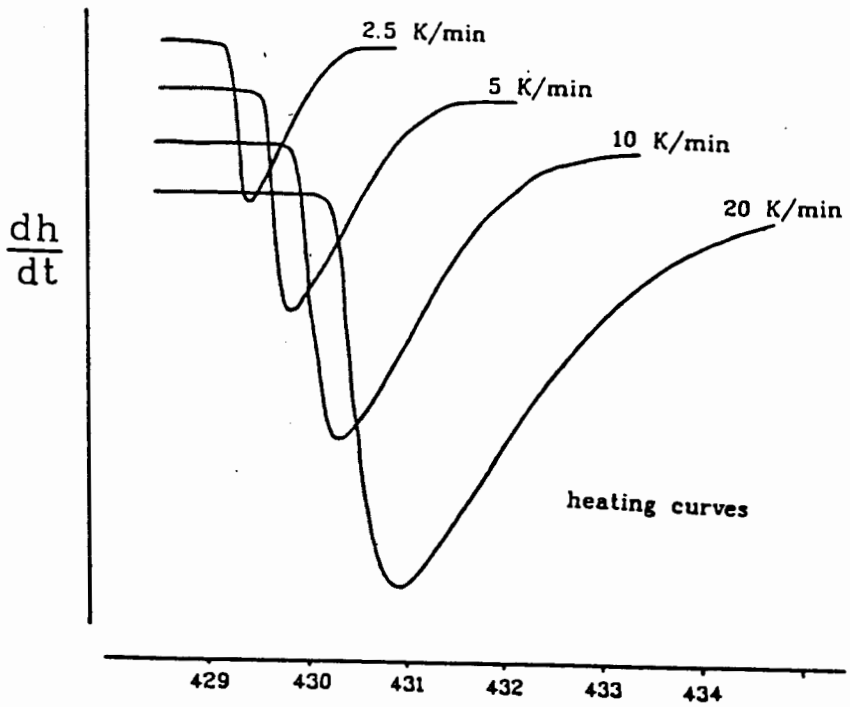

4-7 (a) CELL CALIBRATION COEFFICIENT (E)

The cell calibration coefficient (E) is a conversion factor to convert the differential thermocouple signal from the DSC cell to a differential power. The coefficient (E) is determined from data taken on a sapphire disk and compared to the known values of the specific heat of sapphire at various temperatures. E is given by (66).

$$E = (C * H * m)/(Y * dY) \qquad 4\text{-}11$$

E = cell calibration coefficient

C = heat capacity of the sample at the appropriate temperature

H = programmed heating/cooling rate

m = sample mass

Y = y-axis range setting

dY= (measured difference between heating and cooling curves)/2

The sapphire (Al_2O_3) disk supplied with the equipment was used to determine the cell calibration coefficient (E). Multiple scans were taken with the sapphire calibration sample placed in an aluminum sample pan and an identical empty sample pan used as the reference. The cell calibration

coefficient was determined over the temperature range of 180 K to 360 K by comparing the measured specific heat of Al_3O_2 with the accepted values (66-DSC manual).

Heating and cooling rates of 10 K/min were used for all scans with a low temperature limit of 150 K and high temperature limit of 400 K. The high temperature endpoint of the scan was limited to 400 K to avoid overtaxing the capabilities of the heating unit. The DSC program used is outlined in Appendix III. The difference between the heating and cooling curves were measured at increments of 20 K over the temperature range 200 - 360 K. Measurements between 150 to 180 K in the heating mode and between 400 to 370 K in the cooling mode were not taken because of the time lag for the equipment to equilibriate on starting to heat or cool respectively. The difference between consecutive heating and cooling curves was measured in order to reduce the non-symmetric behavior of the equipment between heating and cooling scans. The cell calibration coefficient was then calculated using the equation 4-11. Three consecutive heating-cooling scans were taken and the results averaged at each temperature in order to eliminate any spurious results and reduce the time dependent characteristics of the equipment when running multiple repetitive scans (such as the build up of frost on the cooling apparatus). The cell calibration coefficient was found to be constant over the latter temperature range (200 - 300 K) having a value of

$E = 0.147 \pm 0.002$ mW/mV.

4-7 (b) Cell Coefficient Check

The heat of fusion of mercury and indium was used to check the cell calibration coefficient (E). Mercury and indium samples were weighed and hermetically sealed in aluminum sample pans. An empty sample pan + lid were used as the reference material for each scan. A strip chart recorder was used to record the transition as a function of time. Heating/cooling rates of 1, 2, 5 and 10 K/min were used. The area of the transition peak was determined by tracing the transition peak with an electronic pen and digitizing tablet coupled to an Apple IIE computer. The cell calibration coefficient (E) was calculated using the equation:

$$E = (H * m)/(A * B * Y) \qquad 4\text{-}12$$

where:

E = cell calibration coefficient

H = heat of fusion of the sample

m = mass of the sample

A = peak area

B = time base setting

Y = y-axis range setting

The average value of the cell calibration coefficient was

found to be 0.144 ± 0.008 mW/mV by averaging the values calculated from heating and cooling scans of the mercury and indium samples using equation 4-12. The value for the cell calibration coefficient as determined from the heat of fusion of mercury and indium agrees with the coefficient determined using the sapphire standard. The value of the cell coefficient (E) used in all subsequent calculations in this thesis is E = 0.147 ± 0.002 mW/mV.

CHAPTER 5

DSC RESULTS

5-1 DSC Procedure

Multiple DSC scans were taken on all Ag_xTiS_2 powder samples (x = 0 to 0.5). Linear heating rates of 5, 10 and 20 K/min were used during the heating phase of the scan and rates of 5 and 10 K/min were used during the cooling phase of the DSC scans. Cooling rates greater that 10 K/min were not obtainable due to the cooling efficiency of the apparatus. The powdered Ag_xTiS_2 samples were placed in small aluminum sample pans having a volume of about 0.06 cc. and sealed with an aluminum lid using the Dupont sample press. Samples weighing between 10 mg. and 40 mg. were sealed in the sample pans. Weights of pristine TiS_2 powder approximately equal to the weights of the sample were sealed in identical sample pans and used as reference materials for the thermal analysis. The samples and reference material were weighed and hermetically sealed in aluminum pans in order to prevent contamination. Pure TiS_2 was used for the reference material in order to maximize the sensitivity of the measurements to the effects due to the silver intercalated in the sample. The DSC program used for investigating the order-disorder transition of the silver in the Ag_xTiS_2 is outlined in Appendix I.

5.2 Specific Heat Measurements of Pure TiS_2

The stock TiS_2 powder was used as a sample material with an empty sample pan and lid used as the reference in a search for any possible transitions in the TiS_2 itself. Data were taken over the temperature range of 100 K to 500 K. The only obvious reproducible transition occurred at 449 ± 2 K during the heating phase and 442 ± 2 K during the cooling phase. The hysteresis in the transition temperature between the heating and cooling runs indicate that the transition may be first order in nature. Todd and Coughlin (66) found a much broader transition involving no isothermal heat absorption but a maximum in the heat capacity near 420 K with the peak slowly decreasing to zero in the range 470 - 520 K, indicating that the transition is second order in nature.

X-ray patterns were taken of the pure TiS_2 samples at 300 K, 450 K, and 550 K in order to determine if any structural changes were associated with the transition observed in the thermal analysis of the TiS_2. Analysis of the Debye Scherrer X-ray data of the pure TiS_2 powders at the latter temperatures (300 K, 450 K, and 550 K) revealed no significant changes in the TiS_2 structure other than the expected small expansion of the lattice parameters at the higher temperatures.

5.3 (a) SAMPLE A (quenched from 800 C). - DSC

There were no detectable transition peaks in the temperature region from 180 K to 440 K for mole fractions of silver less than 0.1 ($x \leq 0.1$). This behaviour is consistent with the supposition of a dilute gas phase in which the silver atoms randomly occupy sites within the layer forming no definite structures. A similar behavior was observed in the X-ray studies done by Scholtz (63).

The calorimetric scans of the samples for which the silver mole fractions were in the range $0.1 < x < 0.25$ clearly indicate transitions occuring at $T = 268 \pm 2$ K for $x = 0.15$ and $T = 272 \pm 2$ K for $x = 0.20$ (Fig. 21a) with the peak height (Fig. 21b) of the transition increasing with increasing mole fraction of silver (x).

Transition peaks occurring at $T = 288 \pm 2$ K were found in all of the samples where the mole fraction of silver was greater than 0.20. The transition temperature ($T = 288$ K) was found to be independent of the silver concentration for $0.25 \leq x < 0.5$ (Fig. 21a) even though there was a double peak for some of the samples ($x > 0.25$ see Fig. 21b). A similar peak shape was observed in the graphite-Br_2 system studied by Culik et. al. (36). The peak height of the transition was observed to increase with increasing silver mole fraction x indicating that the peak and associated transformation are associated with the intercalate. The results of the

Figure 21a

Transition temperature (T_c versus the silver mole fraction (X) for the order-disorder transition for heating the batch A (quenched from 800 C) samples.

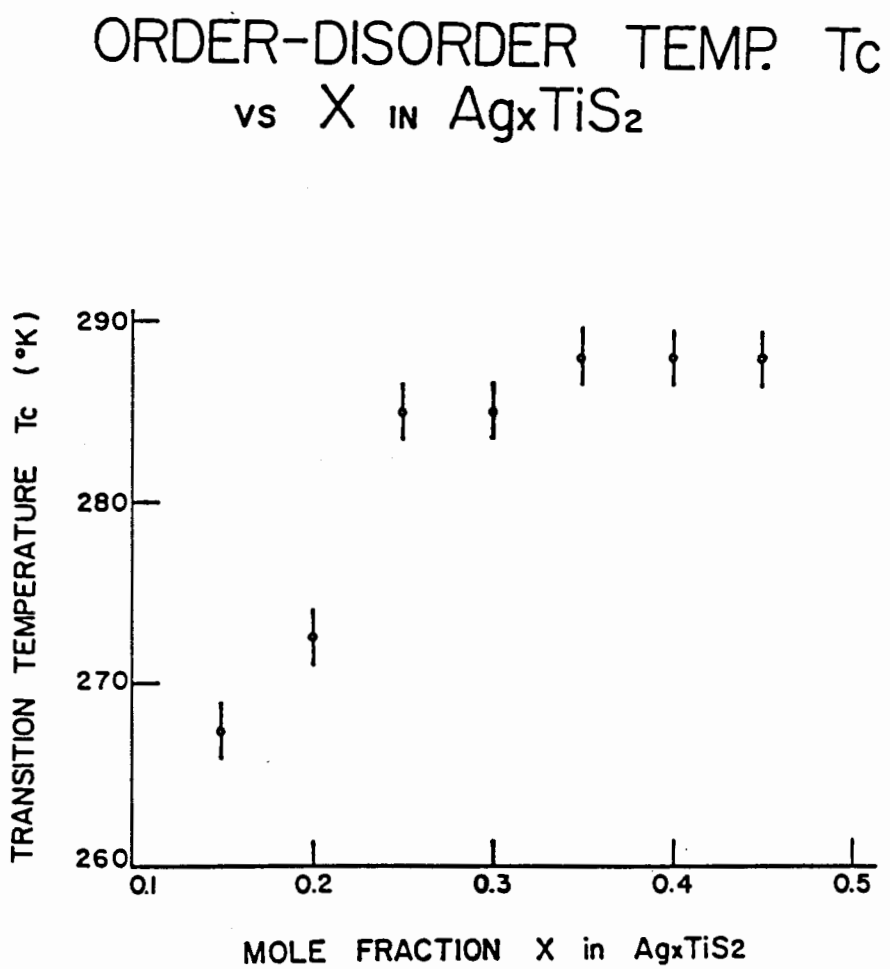

Figure 21b

dH/dT versus temperature for different silver mole fractions (X) from batch A (quenched from 800 C) samples.

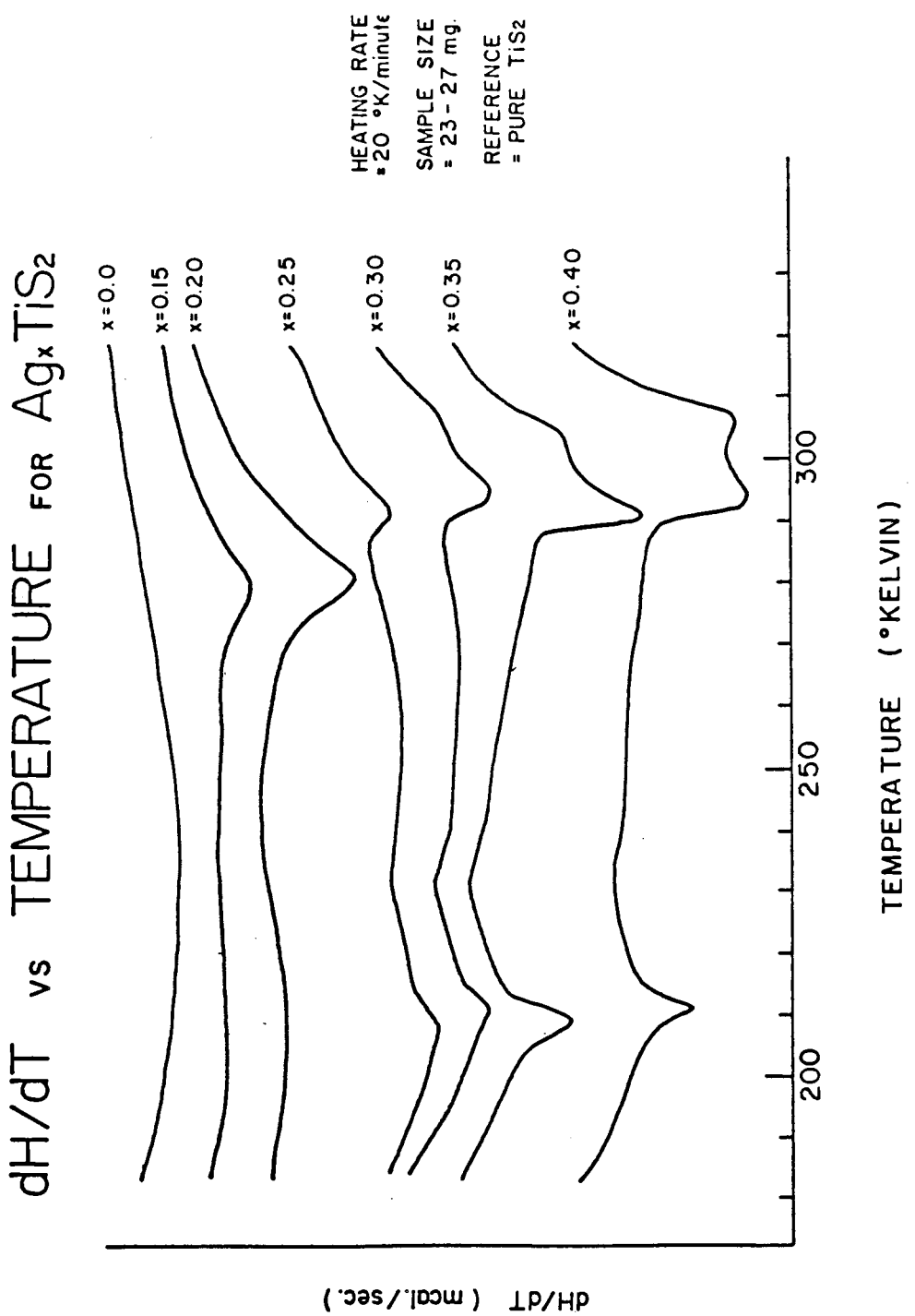

temperature dependence vs. mole fraction of silver intercalate are summarized in Fig. 21a. There was no measureable hysteresis in the temperature of the transition between heating and cooling scans, indicating that there is no isothermal heat absorption. This lack of hystereisis is consistent with previously proposed (22, 23, 65) second order nature of the disorder transition of the silver intercalate. The change in the baseline slope before and after the transition (indicating a change in the specific heat of the sample) in both heating and cooling scans also supports the supposition of a second order transition.

5-3 (b) SAMPLE A (quenched from 800 C). - LOW TEMPERATURE DSC

Calorimetric data of the Ag_xTiS_2 samples (A) obtained in the temperature region from 180 K to 260 K revealed another transition for samples with $x > 0.20$. The program used for the lower temperature scans is outlined in Appendix II. The scans for x 0.35 showed a reproducible transition at T = 208 ± 2 K upon heating (Fig. 21b). Cooling curves were not obtainable due to the lack of cooling efficiency and sensitivity of the equipment. The peak height of the transition was found to increase with increasing mole fraction of silver intercalate indicating that the transition is associated with the silver intercalate.

5-4 (a) SAMPLE B (quenched from 1000 C). - DSC

There were again no distinguishable transition peaks in the temperature range from 180 K to 400 K for silver mole fractions $x <= 0.1$ supporting the supposition of a dilute gas phase for these concentrations. The calorimetric data for samples where $0.1 < x < 0.25$ clearly show transitions occuring at $T = 268 \pm 2$ K for $x = 0.1$ and $T = 272 \pm 2$ K for $x = 0.2$ with the peak height of the transition increasing with increasing mole fraction of silver (x). The transition temperature $T = 288 \pm 2$ K was again found to be independent of the intercalate concentration for silver mole fraction concentrations (x) in the range $0.25 \leq x \leq 0.5$.

A similar behavior was observed in the graphite-Br_2 system studied by Culik et. al. (36). The peak height of the transition was observed to increase with increasing mole fraction x indicating that the peak and associated transformation are due to the intercalate.

The double peak observed in the calorimetric studies of the Group A (quenched from 800 C) samples was not evident in the data taken of the Group B samples (quenched from 1000 C). The results of the temperature dependence vs. mole fraction of silver intercalate are summarized in Fig. 22. Once again (as for the Group A samples quench cooled from 800 C) there was no detectable hysteresis in the transition temperature

Figure 22

dH/dT versus temperature for different silver mole fraction X from batch B (quenched from 1000 C) samples.

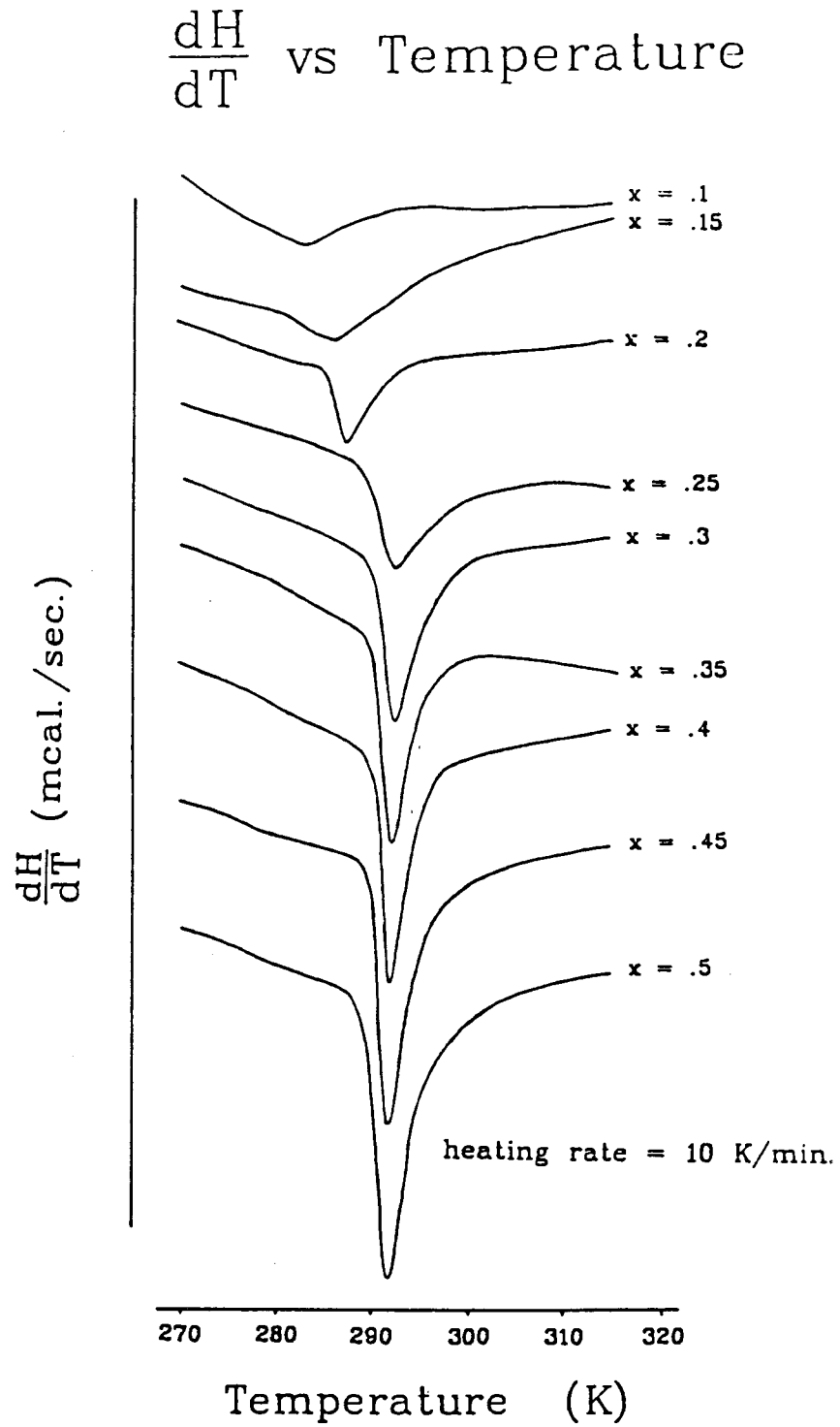

T = 288 K between heating and cooling scans and the baseline behavior was consistent with that expected for a second order transition.

5-4 (b) SAMPLE B (quenched from 1000 C). - LOW TEMPERATURE

Low temperature (180 K < T < 260 K) calorimetric data of the Group B Ag_xTiS_2 samples were similar to the low temperature data from the Group A samples. The scans where $0 < x \leq 0.3$ were devoid of any features that could be associated with a transition while scans for samples with silver mole fraction $x \simeq 0.35$ showed a reproducible transition at T = 208 ± 2 K. The program used for the lower temperature scans is outlined in Appendix II. Cooling curves were not obtainable due to the poor cooling efficiency and sensitivity of the equipment. The peak height of the transition was found to increase with increasing mole fraction of silver intercalate indicating that the transition is associated with the silver intercalate in the samples.

5-4 (c) Low Temp X-ray Patterns - Group B (quenched 1000 C)

Low temperature X-ray diffraction data were obtained from the x = 0.15 and x = 0.20 group B (quenched from 1000 C) samples. Extra diffraction lines were found in the X-ray patterns for $Ag_{0.15}TiS_2$ and $Ag_{0.20}TiS_2$ when the samples were cooled to 150 K. The extra lines were attributed to the formation of a superlattice of Ag atoms within the host TiS_2

lattice. The extra lines were identified as belonging to a $\sqrt{3}a_o \times \sqrt{3}a_o \times c_o$ superlattice (where a_o and c_o are the lattice parameters of the host TiS_2 structure). The ideal occupancy of Ag atoms forming a $\sqrt{3}a_o \times \sqrt{3}a_o$ superlattice is 1/6 for a stage 2 compound and 1/3 for a stage 1 compound although Scholtz (63) reports that the Ag concentration in stage 2 may overfill to $x = 0.20$ and overfill in stage 1 to $x = 0.42$.

5-5 (a) Specific Heat Measurement

The specific heat of the batch B samples (quenched from 1000 C) with silver mole fraction in the range $0 < x < 0.5$ was determined. Sample sizes of 15 to 35 mg. were hermetically sealed in aluminum sample pans and were run against identical empty sample pans in order to cancel the effects due to the spectific heat of the sample pans.

- for measurements far away from the transition regions, equation 4-1 reduces to

$$d/dt(T_S - T_r) = 0 \qquad \text{and} \qquad dh/dt = 0$$

because the sample undergoes no transitions and therefore

$$-(T_S - T_r)/R = (C_S - C_r) * dT_p/dt.$$

In this equation C_S is the specific heat of the sample material plus the specific heat of the sample pan or

$$C_S = C_m + C_r$$

and thus

$$-(T_S-T_r)/R = (C_m+C_r-C_r)*dT_p/dt = C_m*dT_p/dt \qquad 5\text{-}1$$

Equation 5-1 shows that the measured quantity $-(T_S-T_r)/R$ is equal to the specific heat of the sample material (C_m) multiplied by the programmed heating/cooling rate (dT_p/dt) when the reference material is an empty pan identical to the pan containing the sample material and when the sample does not undergo a transition.

5-5(b) Specific Heat Procedure and Results

Three consecutive heating-cooling scans were taken for each sample to eliminate spurious results and reduce the effects of time dependent characteristics of the equipment when running multiple repetitive scans (such as the build up of frost on the cooling equipment).

The specific heat of pure TiS_2 was calculated from the average measured difference between three consecutive heating-cooling scans using equation 5-2.

$$C_m = 60 * E * Y * dy / (2 * H * m) \qquad 5\text{-}2$$

C_m - specific heat of the sample material (when run against an empty pan identical to the pan containing the sample).

E - cell calibration coefficient (mcal/mv).

Y - y-axis range setting (mv/cm).

dy - y-axis deflection (cm).

H - heating rate (K/min).

m - mass of the sample (gm).

5-5 (c) Specific Heat of Pure TiS_2

The specific heat of the pure TiS_2 sample was determined over the temperature range 180 K - 360 K. The results of the measurements are shown in Fig. 23. The values of the specific heat of TiS_2 determined in this work are slightly higher than the values reported by Todd and Coughlin (66), possibly due to an error in the determination of the cell calibration coefficient E of equation 5-2.

5-5 (d) Specific Heat of Ag_xTiS_2

The specific heats of the silver intercalated TiS_2 samples were determined in the same manner as pure TiS_2. The value of the specific heat for TiS_2 was subtracted from the values determined for the Ag_xTiS_2 samples resulting in the

Figure 23

Specific heat of TiS_2 versus temperature.

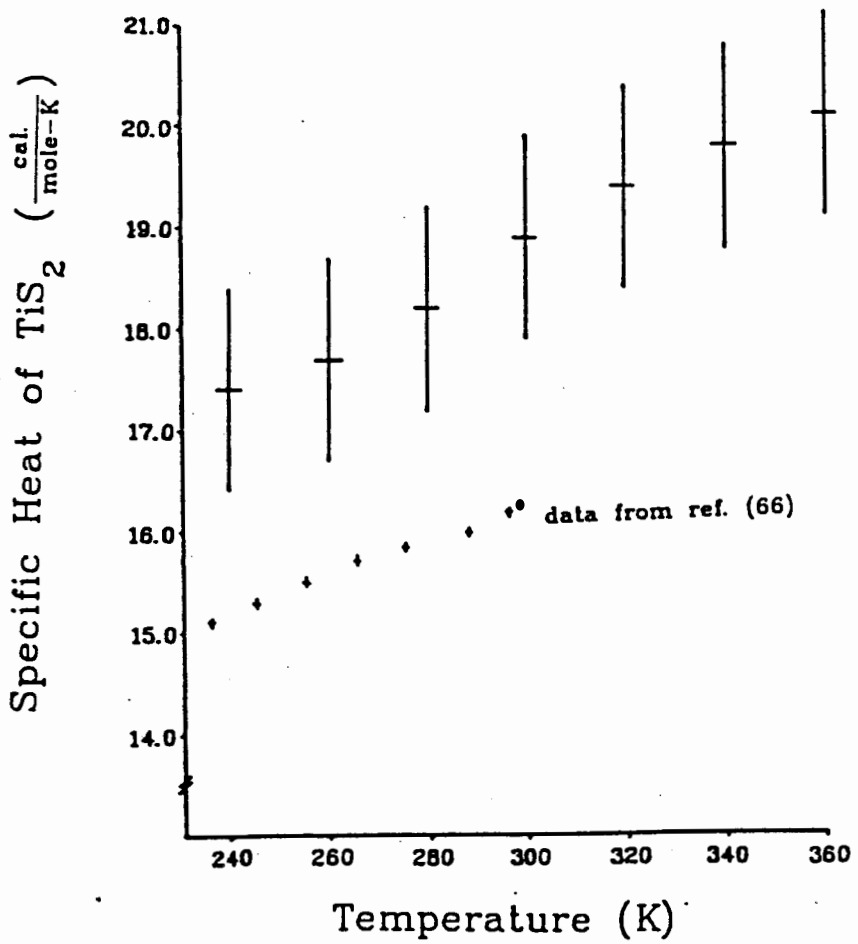

net contribution to the specific heat due to the amount of silver residing in the sample. The contribution to the specific heat due to the silver intercalate is plotted as a function of the mole fraction (x) of intercalate in Fig. 24. The plot Fig. 24 shows the steady increase in C_m as the mole fraction (x) increases from 0 - 0.25 with an change in slope between x = 0.25 - 0.30, then increasing from x = 0.30 to x = 0.50. The transition in the specific heat shown in Fig. 24 for x = 0.25 - 0.30 occurs in the region of pure stage II to pure stage I conversion as indicated by the X-ray data of Section 3.3 (c).

5-5 (e) Specific Heat Comparison with Calculations by Schick et. al. (52)

Given the second order nature of the intercalate order-disorder transition the calorimetric scans yield the variation in the specific heat near T_C. The amplitude and/or area of the peak near T_C can thus be compared, at least qualitatively, to calculations carried out by Schick et. al. (52). They (52) carried out a renormalization group calculation with a triangular Ising model to obtain the variation of C_P near T_C for adsorbed monolayers. Their calculated values were in excellent agreement (52) with measurements carried out on grafoil substrates with submonolayer coverages of He atoms.

The specific heat of $Ag_{0.40}TiS_2$ near Tc has been

Figure 24

Contribution to the specific heat of Ag_xTiS_2 with respect to the sivler mole fraction X at room temperature.

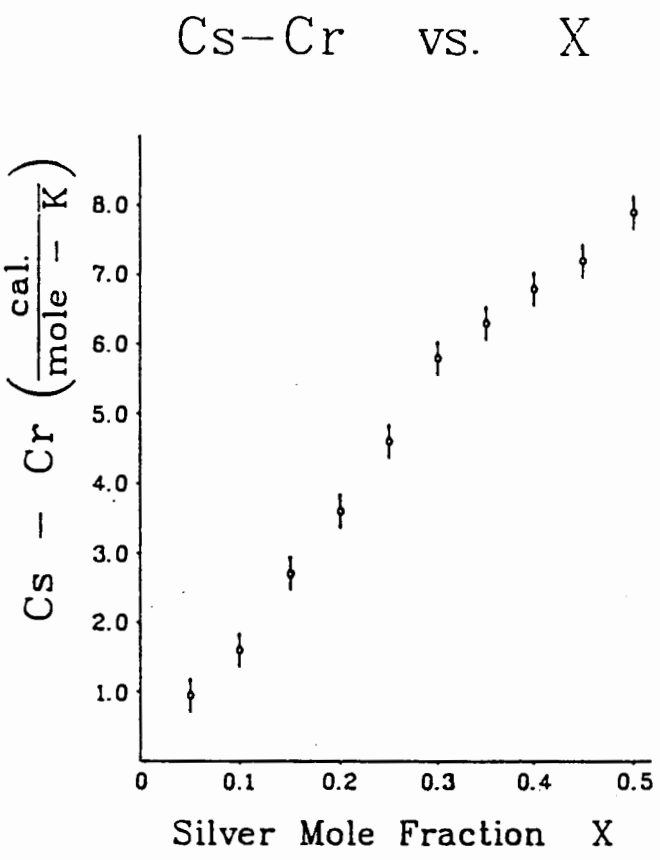

Cs = specific heat of Ag_xTiS_2 sample

Cr = specific heat of TiS_2 reference

measured and a comparison with Schick's theory (52). Fig. 25 shows the measured variation of Cp near Tc and a reproduction of the results calculated by Schick et. al. (52). The area under the experimental peak was determined to be 0.80 and this compares to the value of 0.85 as estimated from the results of Schick et. al. (52). The agreement is perhaps fortuitous in that the measurements were carried out at approximately room temperature and thus there could be significant contributions to the specific heat from other sources. These could include electronic and impurity contributions for example.

Figure 25

Specific heat per particle versus temperature. Thesolid line represents the measured values for $Ag_{0.40}TiS_2$. The dashed line is the results calculated by Schick et. al. (52) for a 0.35 monolayer coverage (taken from Fig. 9 of reference 52).

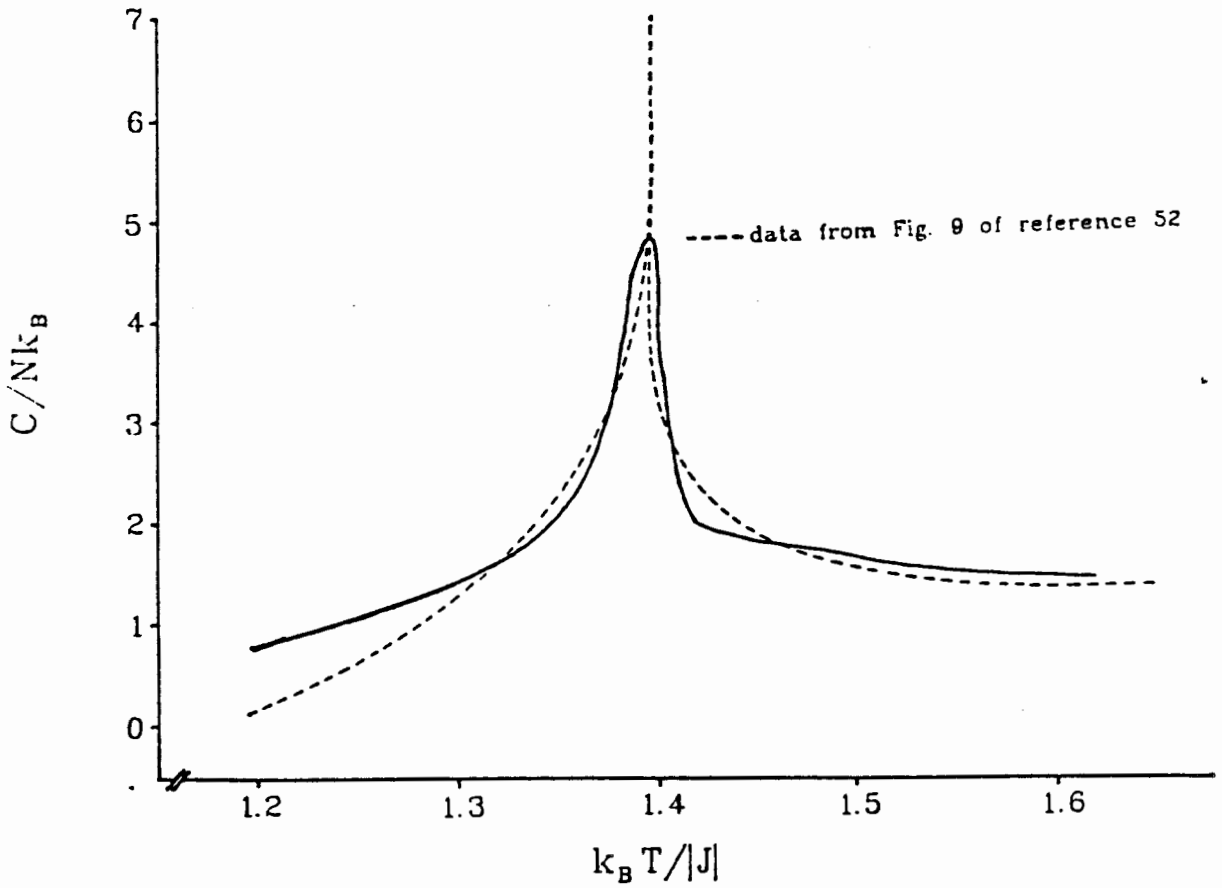

CHAPTER 6

CONCLUSIONS

High quality TiS_2 powders were successfully prepared from the elements. The stoichiometry, structural quality and grain size of the powders were investigated and monitored using X-ray flourescence, X-ray diffraction and electron microscopy techniques.

Differential scanning calorimetry runs were carried out on the Ag_xTiS_2 samples for temperatures in the range $170\ K < T < 600\ K$. The critical temperature Tc for the intercalate order-disorder transition was found to be 268 ± 2 K for $x < 0.15$ (stage 2) and 288 ± 2 K for all concentrations x greater than or equal to 0.20. The independence of Tc of x for $x > 0.20$ could be explained by accumulation of excess Ag in pockets or on the surface. This is also consistent with the invariant appearance of the $\sqrt{3}$ superlattice for all concentrations greater than or equal to 0.15 (21, 22, 31).

There was no observable hysteresis in the critical temperature Tc to within the limits of the experimental accuracy (± 1.0 K). This observation is also consistent with previous observations. Leonelli et. al. (22), Suter et. al. (23) and Plischke et. al. (25) all observed behaviour that led them to conclude that the order-disorder transition was second order in nature. The lack of hysteresis in Tc

corroborates these previous results.

The DSC apparatus was used to measure the specific heat of the unintercalated TiS_2 powders. A value of 17.3 $\pm$ 1.0 cal./mole-K was obtained with the sample at 300 K. This value is in reasonable agreement with the result (16.23 cal/mole-K) obtained previously by Todd and Coughlin (66). Using pristine TiS_2 as a reference, the specific heat of the Ag_xTiS_2 powders was also measured and was found to increase steadily with increasing temperature. The variation in the specific heat near Tc (for x = 0.40) was compared to the results predicted by Schick et. al. (52) for a two dimensional triangular lattice. Good agreement between the two sets of values was obtained.

X-ray diffraction data revealed that the Ag_xTiS_2 powders with $x \geq 0.25$ that were quenched from 800 C consisted of a mixture of stage 1 and stage 2 while similar samples quenched from 1000 C were nominally pure stage 1. This result is also reflected in the calorimetric data where a double peak is observed in the DSC scans of the batch A samples with $x \geq 0.25$. The double peak is postulated to occur because the lower density (stage 2) part of the samples have a transition temperature that is 20 K lower than the stage 1 portion. These samples thus yield two distinct transitions. These results are also consistent with a recently developed staging phase diagram (Bardhan et. al. 68).

Two additional transitions were observed in the course of this work. One was observed in both the pristine and intercalated samples and occurred at T = 449 ± 2 K on heating and 442 ± 2 K upon cooling. A transition in this approximate temperature range had been observed previously (39) but its behaviour was more characteristic of a second order transition. Another transition at 208 ± 2 K appeared in the calorimetric scans of the intercalated samples. There was no evidence of either of the above transitions in X-ray diffraction patterns and the origin of both transitions is unclear.

The nature and physical origin of the transitions at 208 K and 449 K could constitute the subject of future investigations. It would also be of interest to carry out calorimetric measurements on large good quality single crystals of Ag_xTiS_2. The results of such experiments would enable a more detailed comparison with theoretical predictions. Finally, the acquisition of apparatus with high temperature capabilities would enable one to study staging transitions, a subject that is of significant current interest.

APPENDIX

DSC PROGRAM I

1: - cool the sample to 250 K.

2: - hold the sample at 250 K isothermally for 3 minutes to allow the sample to equilibriate at the starting temperature.

3: - heat the sample at 5, 10 or 20 K/min to 330 K.

4: - hold the sample at 330 K isothermatlly for 3 minutes to allow the sample to equilibriate at the high temperature.

5: - cool the sample at 5 or 10 K/min to 250 K.

6: - go to step 2 (repeating the procedure again).

DSC PROGRAM II

1: - cool the sample to 190 K.

2: - hold the sample at 190 K isothermally for 3 minutes to allow the sample to equilibriate at the starting low temperature.

3: - heat the sample at 10 K/min. to 293 K.

4: - hold the sample at 293 K for 3 minutes to allow the sample to equilibriate at the ending temperature.

5: - go to step 1: and repeat the process

BIBLIOGRAPHY

(1) Whittingham, M.S. 1976 J. Electrochem. Soc. 3 (315).

(2) Whittingham, M.S. 1978 Prog. Solid State Chem. 12 (41).

(3) Thompson, A.H. 1978 Phys. Rev. Lett. 40 (1511).

(4) Thompson, A.H. 1979 J. Electrochem. Soc. 126 (608).

(5) Thompson, A.H. 1980 Physica 99B (100).

(6) Dahn, J.R. and Haering, R.R. 1981 Solid State Ionics 2 (19).

(7) Zanini, M., Shaw, J.L. and Tennenhouse, G.J. 1981 J. Electrochem. Soc. 128 (1647).

(8) Weisser, O. and Landa, S. 1973 Sulphide Catalysts, Their Properties and Applications, Pergamon Press.

(9) Schuman, S.C. and Shalit, J. 1971 Catalysis Reviews 4.

(10) Parry, G.S. 1977 Mat. Sci. Eng. 31 (99).

(11) Zabel, H., Moss, S.C., Caswell, N. and Solin, S.A. 1979 Phys. Rev. Lett. 27 (2022).

(12) Leung, S.Y., Underhill, C., Dresselhaus, G. and Dresselhaus, M.S. 1979 Solid State Comm. 33 (285).

(13) Zabel, H. and Magerl, A. 1982 Phys. Rev. B. 25 (2463).

(14) Fuerst, C.D. 1983 Phys. Rev. Lett. 50 (357).

(15) Underhill, C., Leung, S.Y. and Dresselhaus, M.S. 1979 Solid State Comm. 29 (769).

18) Boswell, F.W., Prodan, A. and Corbett, J.M. 1976 Phys. Stat. Sol. 35 (591).

(19) Boswell, F.W., Prodan, A., Vaughan, W.R. and Corbett, J.M. 1978 Phys. Stat. Sol. 45 (469).

(20) De Ridder, R., Van Tendeloo, G., Van Landuyt, J. Van Dyck, D. and Amelinckx, S. 1976 Phys. Stat. Sol 37 (591).

(21) Unger, W.K., Reyes, J.M., Singh, O., Curzon, A.E., Irwin, J.C. and Frindt, R.F. 1978 Solid State Comm. 28 (109).

(22) Leonelli, R. Plischke, M. and Irwin J.C. 1980 Phys. Rev. Lett. 15 (1291).

(23) Suter, R.M., Shafer, M.W. and Horn, P.M. 1982 Phys. Rev. B 26 (1495).

(24) Clarke, R., Caswell, N. and Solin, S.A. 1978 Phys. Rev. Lett. 42 (61).

(25) Plischke, M., Bardhan, K.K., Leonelli, R. and Irwin, J.C. 1983 Can. J. Phys. 61 (397).

(26) Brixner, L.H. and Teufer, B., 1963 Inorg. Chem. 2 (992).

(27) Schafer, H., 1964 Chemical Transport Reactions (Academic Press).

(28) Jellinek, F., 1962 J. less-common Metals 4 9; 1963 Arkiv Kemi 20 (447).

(29) Barstad, J., Gronvold, F., Rost, E., and Vestersjo, E., 1966 Acta chem. Scand. 20 (2865).

(30) Wilson, J.A. and Yoffe, A.D. 1969 Advances in Physics 18 (193).

(31) Sholtz, G.A., 1982 Ph.D. Thesis, Simon Fraser University, Burnaby, B.C.

(32) Kaluarachchi, D.K. 1982 M.Sc. Thesis, Simon Fraser University, Burnaby, B.C.

(33) Whittingham, M.S. 1977 United States Patent 4,007,055.

(34) Whittingham, M.S. 1978 Prog. Solid State Chem. 12 (41).

(35) Daumas, N. and Herold, M.A. 1969 C.R. Acad. Sci., Ser. C. 268 (373).

(36) Culik, J.S. and Chung, D.D.L. 1979 Material Science and Engineering 37 (213).

(37) Leonelli, R. 1977 M.Sc. Thesis, Simon Fraser University, Burnaby, B.C.

(38) Whittingham, M.S. 1981 Mat. Res. Bull. 16 (37).

(39) Mills, K.C. 1974 Thermodynamic Data for Inorganic Sulfides, Selenides, and Tellurides, Butterworths, London.

(40) Parry, G.S., Nixon, D.E., Lester, D.M. and Levene, B.C. 1969 J. Phys. C. 2 (2156).

(41) Winn, D.A. and Steele, B.C.H. 1976 Mat. Res. Bull 11 (551).

(42) Chianelli, R.R., Scanlon, J.C. and Thompson, A.H. 1975 Mat. Res. Bull. 10 (1379).

(43) Whittingham, M.S. and Gamble, F.R. Jr. 1975 Mat. Res. Bull. 10 (363).

(44) Thompson, A.H., Pisharody, D.R. and Koehler, R.F. Jr. 1972 Phys. Rev. Lett. 29 (163).

(45) Scholz, G.A. and Frindt, R.F. 1980 Mat. Res. Bull. 15 (1703).

(46) Berlinsky, A.J., Unruh, W.G., McKinnon, W.R. and Haering, R.R. 1979 Solid State Comm. 31 (135).

(47) Thompson, A.H. Exxon Research and Engineering Company P.O. Box 45, Linden , New Jersey 07036.

(48) Silbernagel, B.G. and Whittingham, M.S. 1976 Journal of Chemical Physics 64 (3670).

(49) Winn, D.A., Shemilt, J.M. and Steele B.C.H. 1976 Mat. Res. Bull. 11 (559).

(50) Thompson, A.H. 1975 Phys. Rev. Lett. 35 (1786).

(51) Dahn, J.R., Mckinnon, W.R., Haering, R.R., Buyers, W.J.L. and Powell, B.M. 1980 Can. J. Phys. 58 (207).

(52) Shick, M. and Walker, J.S. 1977 Physical Review B 16 (2205).

(53) Winn, D.A., Shemilt, J.M. and Steele, B.C.H. 1976 Mat. Res. Bull. 11 (559).

(54) Greenaway, D.L. and Nitsche, R. 1965 J. Phys. Chem. Sol. 26 (1445).

(55) Beal, A.R., Knight, J.C. and Liang, W.Y. 1972 J. Phys. C 5 (3531).

(56) McKinnon, W.R. and Dahn, J.R. 1983 Solid State Comm. 48 (43).

(57) Thompson, A.H., Gamble, F.R. and Symon, C.R. 1975 Mat. Res. Bull 10 (915).

(58) Safran, S.A. and Hamann, D.R. 1979 Phys. Rev. Lett. 42 (1410).

(59) Dahn, J.R., Dahn, D.C. and Haering, R.R. 1982 Solid State Comm. 42 (1979).

(60) Milliman, S.E. and Kirczenow, G. 1982 Phys. Rev. B 26 (2310).

(61) Zunger, A. and Freeman, A.J. 1977 Phys. Rev. B 16 (906).

(62) Moret, R., Tronc, E., Huber, M. and Comes, R. 1978 Phisosophical Magazine B 38 (105).

(63) Jacques, B. and Yves, J. 1963 Adv. in Chem. 39 (191).

(64) Dahn, J.R. and McKinnon, W.R. 1983 J. Phys. C.

(65) Gerards, A.G., Roede, H., Haange, R.J., Baukamp, B.A., and Wiegers, G.A. 1985 Synthetic Metals 10 (51).

(66) Todd, S.S. and Coughlin, J.P. 1952 U.S. Bur. Mines Tech. Paper 525.

(67) Dupont 910 Differential Scanning Calorimeter System Instruction Manual (Part No. 910037000).

(68) Bardhan, K.K., Kirczenow, G. and Irwin, J.C. 1985 J. Phys. C: 18 (L131-L137).
Bardhan, K.K., Kirczenow, G., Jackle, G, and Irwin, J.C. accepted for publication Phys. Rev. B. (Nov. 1985).